STATISTICAL ANALYSIS OF GALAXIES AND CLUSTERS IN SPATIALLY FLAT COLD DARK MATTER UNIVERSE

(Thesis)

Haruhiko Ueda

Uji Research Center, Yukawa Institute for Theoretical Physics, Kyoto University,
Uji 611 Department of Physics, Hiroshima University, Higashihiroshima 724

This is based on the following papers;

Ueda, H., Itoh, M., & Suto, Y. Publ. Astron. Soc. Japan. Vol.45 7 (1993)

Ueda, H., Itoh, M., & Suto, Y. Astrophys. Jarnal. Vol.408 3 (1993)

Ueda, H., Shimasaku, K., Suginohara, T., & Suto, Y. YITP-preprint

ABSTRACT

Spatial distributions and dynamical properties of galaxies and clusters of galaxies are studied in various cosmological models, in order to investigate the dependence of these properties of galaxies and clusters on the density parameter Ω_0 and the dimensionless cosmological parameter λ_0. In accordance with the inflation hypothesis, we confirm ourselves to the spatially flat models with $\Omega_0 + \lambda_0 = 1$. For the dark matter we assume the Cold Dark Matter (CDM) cosmological model which is believed to be most reliable at present. We keep our eye upon this dark matter and estimate these properties numerically.

In order to treat the distribution of galaxies and clusters of galaxies statistically, we first examine the effectiveness of various statistical measure for quantifying the spatial distribution of galaxies. Counts-in-cells and multi-fractal analysis are examined in detail, and are compared with the correlation statistics. A measure similar to the percolation test in count-in-cells analysis provides a useful guide for quantifying the pattern, at least in a complementary manner to the correlation function. We found, however, that it also sensitively depends on the geometry of samples of galaxies. Multi-fractal measures are defined only in a somewhat ambiguous manner due to the discrete nature of galaxy distribution. Then we conclude that although all of them have been successful to some extent in quantitatively describing the pattern of galaxy clustering, none seems to be particularly superior to the two-point correlation function in distinguishing the underlying structure.

Next we examine the distribution of galaxies and clusters obtained to N-body simulation in CDM model in comparison with their observational results. Specifically we consider two spatially flat CDM models: the $\Omega_0 = 1.0$ CDM and $\Omega_0 = 0.2$ CDM model. Galaxies or clusters in these simulations are identified by means of refined friends-of-friends algorithm. We pay attention to the spatial and velocity correlation functions of galaxies and clusters. The overall conclusion is that the $\Omega_0 = 1.0$ CDM model generally fails to reproduce the observed properties of the two-point correlation functions of the clusters, as has been claimed recently in var-

ious independent analyses, while the $\Omega_0 = 0.2$ CDM model is quite successful. In addition to this correlation analysis, we have studied dynamical properties of halos and clusters, by using velocity functions and angular momentum distribution. We found that the $\Omega_0 = 1.0$ CDM simulations reproduce the velocity functions in reasonable agreement with the Press-Schechter theory, but the $\Omega_0 = 0.2$ CDM simulations do not. Quantitative comparison of our velocity functions with the available observational data revealed that only the standard CDM model with a high biasing parameter $b \sim 2$ is consistent with the observation. The distribution of the dimensionless angular momentum λ is very broad ($0.01 \lesssim \lambda \lesssim 0.1$) and the functional form of the distribution looks very universal and is quite insensitive both to the cosmological parameters and to the fluctuation spectral shape. Although the spatial distribution of the angular momentum does not show any noticeable correlation of the orientation, halos with relatively small λ preferentially cluster around dense regions.

From our analysis, it is found that almost all CDM models with the Harrison–Zel'dovich primordial spectrum seem to be ruled out, although the $\Omega_0 = 0.2$ CDM universe is more preferable than the $\Omega_0 = 1.0$ CDM universe. Only the gravitational effect has been so far considered in our analysis, and we have not taken account of other elements, such as the effect of fluidal gas within galaxies and clusters. More statistically reliable observational results and more useful SPH (smoothed particle mesh) simulation models are needed for their detail analyze.

CONTENTS.

1. INTRODUCTION

Selection of a realistic cosmological model, especially the determination of cosmological model parameters Ω_0 and λ_0 is one of the most important problems in modern cosmology. where Ω_0 is the density parameter and $\lambda_0 \equiv \Lambda/(3H_0^2)$ is the dimensionless cosmological constant parameter. We consider this problem through the study of the spatial distribution and dynamical properties of galaxies and clusters of galaxies. As for the constituents of the universe. it is well-known that the almost matter in the universe is dominated by some unknown and invisible particles called "dark matter" (about 95% by mass), and a cold dark matter (CDM) model and a hot dark matter (HDM) model have so far been depending on the particle properties proposed. The CDM model assumes that the dark matter particles were nonrelativistic when they decoupled from the rest of the matter and radiation present in the early universe. On the other hand, the HDM model assumes that the dark matter particles were relativistic at this decoupling time. Structure in the CDM universe form first on smallest scales, and then subsequently larger and larger structures form (bottom-up scenario); structures in the HDM universe form first on a large scale (top-down scenario). The question is which model is better to explain the structure of the universe. The recent positive detection of fluctuations in the cosmic microwave background (CMB) by COBE (Smoot et al. 1992; Wright et al. 1992) supports that the bottom-up picture is basically a successful theory of cosmic structure formation. We then confine CDM models, and keep our eye upon the properties of dark matter.

In this paper we confirm ourselves to the spatially flat models with $\Omega_0 + \lambda_0 = 1$ in accordance with the inflation hypothesis. From this point of view, standard CDM (SCDM) model with $\Omega_0 = 1$ and $n = 1$ was proposed, where n is the spectral index of the primordial density fluctuations. However several difficulties remain to be solved, and most of them are the shape of the primordial density fluctuation spectrum. Once the spectrum shape is given, the COBE result can be used to specify the amplitude of the spectrum. The presence of large-scale

structure seen in the APM angular correlation functions (Maddox et al. 1990) and in the cluster-cluster correlation functions (Bahcall & Soneira 1983; Bahcall 1988) require large-power of fluctuation spectrum on large scales. On the other hand, the large-scale coherent velocity field (Dressler et al. 1987), and the very cold velocity flow of galaxies on small scales (Ostriker & Suto 1990; Suto, Cen, & Ostriker 1992; Strauss, Cen, & Ostriker 1992) indicates that fluctuation of small-scale power should be quite small. The SCDM model cannot account for the above situation in a consistent manner. Ostriker & Suto (1990) is the first to argue in a quite generic context that the available observational data are reconciled only by relaxing the standard assumptions and accepting that $\Omega_0 < 1$ and/or $n < 1$. Subsequent works by Suto, Gouda, & Sugiyama (1990) and Suto & Suginohara (1991) expressed the need for the condition $\Omega_0 < 1$ and/or $n < 1$ more specifically using the quantitative theoretical analysis of one-dimensional pair-wise velocity dispersions and the microwave background anisotropies. It should be noted here that the spectrum with $n = 1$ had been suggested by Harrison (1970) on the basis of a phenomenological argument, and the inflationary model (Guth 1981) also supports this relation. Moreover $\Omega_0 < 1$ is suggested by observation, so we consider pursue the $\Omega_0 < 1$ CDM (LCDM) model without imposing the condition $n \neq 1$. For taking the low density models, we consider the bias effect apparently when we discriminate gravitating inhomogeneity and luminous inhomogeneity. Then in addition to LCDM case, we also treat SCDM with $b_\rho > 1$ where b_ρ is the spatial biasing parameter.

In general, the non-liner effects will decrease the reliability of the analytical relations between the density parameter and spatial, dynamical properties of galaxies and clusters. On the other hand, cosmological N-body simulations have proved to be a powerful and reliable means in quantitatively exploring several specific predictions. Therefore we investigate the properties of galaxies and clusters in spatially flat CDM universe by performing a series of cosmological N-body simulations. In order to study the properties of galaxies and clusters statistically, we first

examine the usefulness of various measures by which we characterize the spatial distribution of galaxies in the present universe. Perhaps the two-point correlation function (Totsuji and Kihara 1969) is the most famous statistical measure used for the galaxy clustering. Count-in-cell and multi-fractal analysis have also been proposed by various authors, but the usefulness of these measures has not been examined sufficiently. We then examine in detail these two measures regarding large-scale structure and judge what is the most useful measure to quantifying the spatial distribution of galaxies.

After examining the usefulness of statistical measures, we then investigate the spatial distribution and dynamical properties of galaxies and clusters of galaxies predicted in the CDM models, paying particular attention to the value of Ω_0. As was stated before, we mainly attempt to clarify the difference between SCDM with $b_\rho > 1$ and LCDM. In order to examine the properties of clusters, we have to define clusters in N-body simulations. Our particle grouping method is based on the adaptive linking method (ALM) developed by Suto, Cen, & Ostriker (1992), and also used in Suginohara & Suto (1992), Ueda et al. (1993), and Watanabe et al. (1993). The method refines a conventional friends-of-friends algorithm which assumes the constant linking length, and uses the variable linking length instead, as will be shown in §2. One of the most important issues concerning the spatial distribution of clusters is the amplitude of the cluster-cluster two-point correlation function $\xi_{cc}(r)$. The observed amplitude of $\xi_{cc}(r)$ is larger than that of galaxy-galaxy correlation function $\xi_{gg}(r)$. In addition, the analysis in §3 confirms that the correlation statistic is the most reliable statistical measure to characterize the pattern of galaxy distribution. Then we examine the correlation functions of clusters and see which of SCDM and LCDM reproduces observational results or not.

In addition to this correlation analysis, we also examine the dynamical properties of galaxies and clusters from the stand point of velocity function and angular momentum. The velocity function (VF) is defined as the number density of objects as a function of their circular velocity. This is directly observable as in the lumi-

nosity function, while it is difficult to derive a reliable estimate of the dynamical mass of distant astronomical objects, and the mass function has been poorly determined in general. In contrast to the luminosity function, on the other hand, one can predict the specific model for the velocity function in a straightforward manner without requiring proper understanding of star formation in the objects. Therefore VF is better than the other two in confronting the model prediction with the observations, and the comparison will have more reliable and direct implications on the model. In addition to this VF analysis, we try the statistical analysis for spatial distribution of angular momenta of galaxies and clusters. By using these results, we also investigate which of SCDM and LCDM reproduces observational results.

The rest of the paper is organized as follows: The results of N-body simulations and the grouping scheme to identify galaxies and clusters of galaxies are described in §2. The usefulness of various measures is examined in §3. In §4, the spatial distributions of galaxies and clusters of galaxies are studied, and their dynamical properties of them are examined in §5 by computing the velocity function and angular momenta. Finally in §6, we summarizes our main conclusions.

2. SIMULATION DATA AND IDENTIFICATION CRITERION

In this paper, we examine the properties of galaxies and clusters of galaxies in spatially flat CDM universe on the basis of their spatial and velocity distributions derived in cosmological N-body simulations. These N-body simulations are evolved using a hierarchical tree code with the fully periodic boundary condition in a cubic volume of L_b^3 (Hernquist, Bouchet, & Suto 1991; Suginohara et al. 1991). In each section, different models are used which are summarized in Table 1. The detailed informations of our simulation models are shown in the following;

As is stated in §1, we are mainly interested in the CDM model with $\Omega_0 < 1$ or $b_\rho > 1$, so we take the LCDM model with $\Omega_0 = 0.2$ and $\lambda_0 = 0.8$, and the SCDM model with $\Omega_0 = 1.0$, $\lambda_0 = 0.0$ and the biasing parameter $b_\rho = 1.7$. The amplitudes of the spectrum of density perturbation are normalized by using the galaxy-galaxy two-point correlation functions. For SCDM the real-space correlation function of galaxies cannot be expressed in the form of a single power-law so well. A marginally good fit is obtained for $h \equiv H_0/(100\,\mathrm{km\,s^{-1}\,Mpc^{-1}}) = 0.42 \pm 0.02$ for 1.7σ peak particles. For simplicity, however, we use $h = 0.5$ in SCDM instead, and this makes the correlation length of galaxies in the simulation slightly smaller than the observed value. The LCDM model gives a good match to the observed galaxy-galaxy correlation function for $b_\rho = 1$. These details would not change the main conclusions in the present paper. In order to examine the properties of galaxies and clusters, we prepare many models with different scale. We call our CDM models as GS, GL, CS, and CL, where G and C stand for galaxy and cluster scales while S and L stand for SCDM and LCDM models. In addition, the subscript number of each CDM model represents the simulation boxsize L_b in order to show the difference between models clearly.

In addition to CDM models, we also adopt the power-law models which start from initially scale-free density fluctuations (Suginohara et al. 1991). To be more specific, the power spectrum of those models obeys the following form:

$$P_{\rm init}(k) \equiv \langle|\delta_{\mathbf{k}}|^2\rangle_{\rm init} = \frac{A_i}{N}\left(\frac{k}{k_{\rm N}}\right)^n, \qquad (n = -2,\ -1,\ 0,\ \text{and}\ 1) \tag{2.1}$$

where $\delta_{\mathbf{k}}$ is the Fourier transform of the density contrast, $\langle\ \rangle$ denotes an ensemble average, N is the number of particles employed in the simulations, $k_{\rm N} \equiv \pi N^{1/3}$ is the Nyquist wavenumber corresponding to the mean particle separation, and A_i is the input amplitude. We call these as $n = -2,\ -1,\ 0,\ 1$ model. These four models are evolved in the Einstein-de Sitter universe with density parameter $\Omega_0 = 1$ and the Hubble parameter $h = 1$.

In §3, we test the usefulness of the measures used to quantify the pattern of the galaxy distribution. In order to do this, we prepare for $n = 1,\ 0,\ -1,\ -2$ power-law models and GL_{100} model. All of these five simulations employ $N = 262,144$ particles, and the mass of an individual particle in GL_{100} model is $2 \times 10^{11} M_{\odot}$, roughly equal to a typical galactic mass. Although power-law models have no typical scale, we suppose that each particle in our simulations corresponds to a galaxy.

In §4 and 5, we identify *galaxies* and *clusters of galaxies* in the CDM simulation data in the specified method, in order to examine the dynamical properties of these objects. We adopted an adaptive linking method (ALM) to identify galaxies and clusters in the simulation data. ALM refines the more conventional Friends-of-Friends algorithm which assumes the constant linking length, and uses the variable linking length b_{ij} between i-th and j-th galaxies depending on the local density. More precisely, b_{ij} is defined as

$$b_{ij} = \mathrm{Min}\left[\frac{L_b}{N^{1/3}}, \frac{\beta}{2}\left(\frac{1}{n_i^{1/3}(r_s)} + \frac{1}{n_j^{1/3}(r_s)}\right)\right], \tag{2.2}$$

where

$$n_i(r_s) \equiv \frac{1}{(2\pi r_s^2)^{3/2}} \sum_{l=1}^{N} \exp\left(-\frac{|\mathbf{r}_i - \mathbf{r}_l|}{2r_s^2}\right). \tag{2.3}$$

is a local density of i-th galaxy and $\mathbf{r}_i$ is a position vector of the i-th galaxy. After the particles were properly grouped, we removed particles which are not gravitationally bound, but this additional procedure hardly changes the results below. The ambiguous point of this method is how to determine the set of parameters $(r_s,\ \beta)$. In fact we do not know how to determine the suitable set. To find some clue, we compare the resulting mass function of the identified clumps with that indicated from the observed luminosity functions of galaxies and clusters of galaxies $\phi(L)$. If the mass-to-light ratio is independent of L, we estimate the mass function of galaxies and clusters in the universe. Then we determine the suitable set of

parameters in order to compute the mass functions of our clumps. Still it is not clear if the resulting groups can be regarded as realistic galaxies or clusters in our universe. With this in mind, we will call *halos* and *clusters* referring to the groups of particles in our models in §4 and §5 respectively.

3. USEFULNESS OF VARIOUS MEASURES FOR QUANTIFYING SPATIAL DISTRIBUTIONS OF GALAXIES

The main purpose of this section is to select a good statistical measure by which can distinguish the different patterns of particle distributions. We mainly pay attention to the following three analysis; Two-point correlation function analysis (§3-1), Count-in-cell analysis (§3-2), Multi-Fractal analysis (§3-3). In order to perform this analysis, we use the $n = 1, 0, -1, -2$ power-law models and GL_{100} model whose galaxy distributions are shown in Figure 1. These figures show the x-y projection of particles situated between $-L_b/20 \leq z \leq L_b/20$. Before examining the usefulness of these measures, we first compare these models according to a visual impression. From these figures, we can easily recognize the difference among the five models from our eyes: many small (large) clusters are abundant in the $n = 1$ ($n = 0$) model, while in the models of $n = -1$ $n = -2$ and GL_{100} the mutually connected filamentary structures are prominent. In fact, the initial power spectrum of GL_{100} model can be roughly approximated by an effective power-law index in the -1.7. Therefore the general feature of GL_{100} model appears to be fairly similar to the $n = -1$ and $n = -2$ models. In the following, we examine whether the above statistical measures property quantify galaxy distribution pattern of these models or not.

3-1. Two-point Correlation Function Analysis

The two-point correlation function, $\xi(r)$, has been most widely used for statistically describing the galaxy clustering (Totsuji and Kihara 1969; Peebles 1980). The two-point correlation function is defined by the probability of finding an object in both of the volume elements δV_1 and δV_2 at a separation r

$$\delta P = \bar{n}^2 \delta V_1 \delta V_2 [1 + \xi(r)], \tag{3.1}$$

where $\bar{n}$ is a mean number density of object. From this equation, one can easily notice that $\xi(r)$ represents the deviation from the uniform distribution. Because the distributions of galaxies in different models are evolved with different initial spectra, the different galaxy distribution patterns are caused by different deviations from a uniform distribution. Therefore the correlation statistic is expected to distinguish the pattern property. The results of two-point correlation functions are plotted in Figure 2, and these behaviors are in agreement with the visual impression in Figure 1a-1e; the $n = 1$ model shows a rapidly decreasing correlation compared with others, reflecting that the correlation in the model is small on large scales. The clustering in the $n = 0$ model is the strongest among the five. This situation is clear from the amplitude of $\xi(r)$ on very small scales. The correlation functions for $n = -1$ and GL_{100} appear to be fairly similar, again in reasonable agreement with the visual impression from Figure 1. The structure in the $n = -2$ model exhibits a strong coherence over the entire simulation box; this is manifest in the largest amplitude of $\xi(r)$ for $r/L_b \geq 0.02$ among the five models. The slope and correlation length, r_0, where $\xi(r)$ is unity (see (4.1)), are summarized in Table 2. Anyway, the two-point correlation function is a desirable measure to describe the spatial distribution of galaxies property.

3-2. Count-in-Cell Analysis

In the count-in-cell method, we divide the entire sample into M^3 regular grids, and then computes the number of particles in each cell. By examining the statis-

tical properties of the distribution of the counts in cells, one might quantify the underlying spatial pattern in the sample. Here we consider two new measures.

The first measure concerns a basic question regarding the dimensionality of patterns in galaxy distribution. We briefly describe the procedure of this analysis first. We define the expectation number of particles per cell, n_{exp}, as

$$n_{exp} = \frac{\text{total number of particles}}{\text{total number of cells}} = \frac{N}{M^3} = N\left(\frac{\epsilon}{L}\right)^3, \tag{3.2}$$

where $\epsilon \equiv L/M$ is the size of each cell. A cell is called "occupied" if it contains at least one particle, and the expectation number of particles in the occupied cells, n_{occ}, is defined by

$$n_{occ} = \frac{\text{total number of particles}}{\text{total number of occupied cells}}. \tag{3.3}$$

Both n_{exp} and n_{occ} are functions of the total number of cells M^3 or the size of each cell ϵ. From the CfA galaxy redshift slice data, de Lapparent et al. (1991) found that the above quantities approximately obey the following simple law:

$$n_{occ} - 1 = K n_{exp}^{\beta/3} \tag{3.4}$$

with $K \sim 2$ and $\beta \sim 2$. The value of β is interpreted as being an average dimensionality of structure. In this method, K and β are measures to characterize galaxy distribution, and we here apply this method to our models which are shown in Figure 3. In fact, for $n_{exp} \lesssim 10$ the behavior of $n_{occ} - 1$ against n_{exp} is approximated by a single power law, like equation (3.4). The least-square fitted values for K and β in the range of $n_{exp} \leq 1.0$ are summarized in Table 2. Although the value of β systematically increases from the $n = 1$ model to the GL_{100} model, in agreement with the visual impression, all of them are close to unity in spite of the apparently different pattern shown in Figures 1a to 1e. The value of β is meaningful only in the sense of an "average" dimensionality. Our main conclusion here is that β is not

sensitive to the pattern of structure and, moreover, does not seem to properly represent the dimensionality of the typical structure. This is ascribed to the fact that β represents the "average" dimensionality of structure; the real pattern does not comprise pure rods or sheets, but a mixture of various geometrical structures. Such information is simply smoothed out by the simple analysis based on equation (3.4). The amplitude K seems to represent the fluctuation amplitude on small scale. We found that the $n = 0$ model has the largest K, while the $n = -1$, -2 and GL_{100} models result in a similar value (~ 3); this tendency is in good agreement with the behavior regarding $\xi(r)$ for $r \lesssim 0.01L$. Note that the scale r should approximately correspond to $(n_{exp}/N)^{1/3}L$. The fact that the value of K in the GL_{100} model is closest to the observed value (~ 2.0) is explained by the fact that the model reproduces very well both the amplitude and shape of the observed correlation. Therefore, K does not seem to contain any more information than that contained in $\xi(r)$. Moreover, the cells with $n_{exp} \lesssim 1$ are dominated by either the shot noise or the discrete nature of the particle distribution. It is therefore necessary to properly normalize the number density of galaxies in order to confront the observed data.

The second measure called "filling factor" is related to the percolation analysis. Any two occupied cells whose sides, ridges or corners are connected with each other, are regarded as being members of a 'system' of linked cells. The quantity f_{per} is defined as

$$f_{per} = \frac{\text{volume of the largest system}}{\text{total volume of occupied cells}}. \tag{3.5}$$

This is negligible small when the size of the cell, ϵ, is small. As ϵ becomes larger, the volume fraction of the occupied cells,

$$f_{occ} = \frac{\text{total volume of occupied cells}}{\text{total volume of cube}}, \tag{3.6}$$

increases, and then several systems merge and form a bigger system. The filling factor, F, is defined as the value of f_{occ} where f_{per} is 0.5. Figure 4 plots f_{occ} against f_{per}; the resulting filling factors are summarized in Table 2. The values

of F decrease systematically according to the clustering pattern in the models. We found, however, that the shape of the curves is more suited to distinguish the features of the underlying pattern. The slopes of the curves become less steep as the large-scale coherence in the models becomes manifest. Note that a small f_{occ} corresponds to the small-scale structure, while a large f_{occ} represents the large-scale behavior of the pattern in each model. Figure 2 shows that the $n = -1$ and GL_{100} models have almost identical $\xi(r)$ for $r/L \lesssim 0.01$, while their $f_{occ} - f_{per}$ curves are distinct for $f_{occ} \lesssim 0.07$. On the other hand, the $n = -2$ and GL_{100} models have fairly similar $f_{occ} - f_{per}$ curves, whereas the amplitudes of their $\xi(r)$ are different (although their slopes are quit similar). We therefore conclude that the $f_{occ} - f_{per}$ curve is potentially a very useful measure for quantifying the pattern, and is in fact, complementary to $\xi(r)$. In particular, the gradual increase of the curves for the $n = -1$ and GL_{100} models, rather than the rapid rise seen in the $n = 1,\ 0,\ -1$ models, clearly indicates the presence of a strong coherence intrinsic to the particle distribution. The filling factor, on the contrary, contains rather limited information, and differs sensitively to the specific definition, as is clear from the shape of the curves in Figure 4. We further examine the geometrical dependence of the $f_{per} - f_{occ}$ curves, and found that this is very sensitive to the shape of the original sample. This dependence is not problematic as a quantitative measure of the cosmological structure, but, rather, requires caution in inferring the pattern of the universe from an analysis of limited observed data.

3-3. Multi-Fractal Analysis

The failure of the average dimensionality β comes from averaging the dimensionality over the entire sample. This averaging process loses a significant fraction of the information. Same difficulty appears in a simple fractal approach which one attempts to characterize galaxy clustering by means of a single fractal dimension. This naturally leads to a generalization of the simple fractal, i.e., the multi-fractal analysis.

We briefly introduce several basic quantities in performing a multi-fractal analysis. (Further details can be found in Jones et al. (1988), Martinez et al. (1990) as well as Itoh (1990)). The generalized dimension D_q is defined by

$$D_q = \frac{\tau(q)}{q-1}, \tag{3.7}$$

where q is an arbitrary real number,

$$\tau(q) = \lim_{\epsilon \to 0} \frac{\log \sum_i [p_i(\epsilon)]^q}{\log \epsilon}, \tag{3.8}$$

with

$$p_i(\epsilon) = \frac{n_i(\epsilon)}{N} \tag{3.9}$$

being the cell occupancy probability. If all of the D_q's are equal, the distribution is called a 'simple' fractal. In a general system, however, they are different and, indeed, one can prove that $D_{q'} \geq D_q$ when $q' < q$. The evaluation of D_1 directly from equation (3.7) is problematic, though it is easy to show that equations (3.7) and (3.8) reduce to

$$D_1 = \lim_{\epsilon \to 0} \frac{\sum_i p_i \log p_i}{\log \epsilon} \tag{3.10}$$

for $q \to 1$, which was used in our analysis. A delicate and intrinsic problem is related to the procedure of $\epsilon \to 0$ in the above definitions. Since we are dealing with a distribution consisting of discrete particles, the limit is not well defined. We therefore decided to perform a multi-fractal analysis while explicitly keeping the ϵ dependence

We now examine the generalize dimension of our models which are shown in Figures 5a to 5c. These results are plotted so as to show the model dependence for $\epsilon = 1/100$, $1/500$, and $1/1000$, respectively. The difference shows up only for

$q \geq 0$, which preferentially weights the overdense cells and, thus, should represent mainly small-scale nonlinear clustering. Although the behavior of D_q as a function q is distinguishable, the model-to-model difference is significantly dependent on the value of ϵ. It is also clear from Table 2 that the values of D_q are not sensitive to the model compared with the strong ϵ dependence. It therefore seems to be difficult to draw any secure conclusion from this analysis, taking into account the difficulty that one cannot take the $\epsilon \to 0$ limit properly. (There exists other definitions of generalized dimension to avoid $\epsilon \to 0$ limit. In this case, we found that the partition function is a good measure to quantifying galaxy distributions. But we also found that this has a geometrical dependence. In addition, it is necessary that there are sufficient galaxy informations to estimate partition function, and we conclude that multi-fractal analysis is not superior to the two-point correlation function (Ueda 1993)).

4. CORRELATION FUNCTION ANALYSIS OF GALAXIES AND CLUSTERS IN SPATIALLY FLAT CDM MODELS

As is stated in introduction, our main purpose is to determine cosmological parameters under the flat CDM model. Spatial distributions of galaxies and clusters depend on the density parameter Ω_0, and so the comparison of the cluster distributions in N-body simulation of SCDM and LCDM with observation gives us a useful information about Ω_0. From the result in §3, the correlation analysis is the most promising measure to quantify the galaxy spatial distribution. Accordingly we quantify spatial distribution of galaxies and clusters with two-point correlation function (§4-1). In addition to the spatial distribution, velocity distribution of galaxies and clusters bring also an important signal to determine cosmological pa-

rameters, and we also examine this by using the correlation statistics (§4-2). The CDM models which are used here are CS_{130} and CL_{100}.

4-1. Two-point Correlation Functions of Clusters

Davis & Peebles (1983) showed that the observational galaxy-galaxy two-point correlation function $\xi_{gg}(r)$ is expressed approximately as

$$\xi_{gg}(r) = \left(\frac{r}{r_0}\right)^{-1.8}, \qquad r_0 = 5.4h^{-1}\mathrm{Mpc}. \tag{4.1}$$

It is known that the SCDM model with biasing parameter $b_\rho = 1.7$ or the LCDM model can reproduce this relation.

The cluster-cluster two-point correlation function $\xi_{cc}(r)$ is also expressed approximately as that of $\xi_{gg}(r)$, but the correlation length of $\xi_{cc}(r)$ from the analysis of the Abell clusters (Bahcall & Soneira 1983) is larger than that of $\xi_{gg}(r)$. One of the well-known problems in the SCDM model (White et al. 1987) is that it cannot reproduce this high amplitude of the cluster-cluster correlation function $\xi_{cc}(r)$. Bahcall (1988) and more recently Bahcall and West (1992) found that the correlation lengths are approximately proportional to the sample's mean separation d_i, where the index i refers to the system being considered, and proposed a universal correlation function in the form :

$$\xi_i(r) = \left(\frac{r}{r_{i,0}}\right)^{-1.8}, \qquad r_{i,0} = (0.4 \sim 0.5)d_i. \tag{4.2}$$

If we take into account that the amplitudes of the cluster-cluster correlation functions depend on the definition of the clusters itself in the observed samples, the available data from the Abell, APM, and Durham-Edinbough catalogs can be in reasonable agreement (Bahcall & Soneira 1983; Dalton et al. 1992; Nichol et al. 1992; N.A.Bahcall, in private communication).

We here estimate the cluster-cluster two-point correlation function in the SCDM and LCDM models, and examine which of SCDM and LCDM can reproduce the observational results expected in equation (4.2). Figures 6a and 6b show the two-point correlation functions in real space $\xi(r)$ of galaxies (curves) and of clusters (symbols), while those in redshift space $\xi(s)$ are plotted in Figures 6c and 6d. In these figures, we employed all the clusters of $M > 7.4 \times 10^{13} M_\odot$ (SCDM) and $M > 2.7 \times 10\ 13 M_\odot$ (LCDM), just for an illustrative purpose. In order to elucidate the dependence of the 'definition' of clusters, we calculated the correlation functions of clusters with different mass ranges. Then we found that the amplitude of $\xi_{cc}(r)$ does increase as the mass of the cluster increases. Due to the limitation in the simulation box size L_b, the number of clusters is small especially for large clusters and thus the error bars are relatively large. Nevertheless $\xi_{cc}(r)$ is consistent with a power-law form around $\xi_{cc}(r) \sim 1$. To be more precise, we made a χ^2-fit of the results to a power-law form in $0.3 \lesssim \xi \lesssim 3$ and listed the correlation lengths of galaxies and clusters ($r_{g,0}$, $r_{c,0}$ in real space and $s_{g,0}$, $s_{c,0}$ in redshift space†), and the power-law index γ in Table 3. In this table, we choose three types of the criterion for masses of clusters. In order to show the relation between the correlation length and the mean separation length more clearly, we made a χ^2-fit for our results which are shown in Figure 7. A straight line in this figure shows that

$$\begin{aligned} r_{c,0} &= (0.28 \pm 0.02)\ d + (1.5 \pm 0.2) \quad (\chi^2 = 0.09), \\ s_{c,0} &= (0.28 \pm 0.02)\ d + (2.1 \pm 0.2) \quad (\chi^2 = 0.02), \end{aligned} \qquad \text{(SCDM)} \qquad (4.3)$$

and

$$\begin{aligned} r_{c,0} &= (0.45 \pm 0.01)\ d + (2.2 \pm 0.2) \quad (\chi^2 = 0.01), \\ s_{c,0} &= (0.36 \pm 0.03)\ d + (4.2 \pm 0.4) \quad (\chi^2 = 0.1). \end{aligned} \qquad \text{(LCDM)} \qquad (4.4)$$

† Kaiser (1987) and Suginohara & Suto (1991) explained the larger correlation lengths in redshift space in linear theory.

When we fitted to a power-law model instead, we obtained

$$\begin{aligned} r_{c,0} &= (1.1 \pm 0.05)\ d^{0.59\pm0.02} \quad (\chi^2 = 0.03), \\ s_{c,0} &= (1.5 \pm 0.03)\ d^{0.52\pm0.01} \quad (\chi^2 = 0.001), \end{aligned} \qquad \text{(SCDM)} \qquad (4.5)$$

and

$$\begin{aligned} r_{c,0} &= (1.2 \pm 0.06)\ d^{1.2\pm0.06} \quad (\chi^2 = 0.01), \\ s_{c,0} &= (1.4 \pm 0.4)\ d^{0.7\pm0.1} \quad (\chi^2 = 0.8). \end{aligned} \qquad \text{(LCDM)} \qquad (4.6)$$

Note that the cluster-cluster correlation becomes significantly larger in both models than in all simulation particles case, and the fits made to the clusters in equations (4.3) and (4.4) seem to be extended naturally to the correlations of the galaxies. Although the errors are relatively large, the observed correlation amplitude is reproduced in LCDM, but not in SCDM. This is due to the fact that LCDM has more fluctuation powers on large scales than SCDM. We then conclude that the $\Omega_0 < 1$ model (with/without nonzero λ_0) is better than the $\Omega_0 = 1$ model.

4-2. Velocity Correlation Functions of Galaxies and Clusters

Velocity fields of galaxies and clusters also give us important informations about the density parameter Ω_0. Peculiar velocity fields in galaxies and clusters can be statistically described by the velocity correlation tensor (Górski et al. 1989; Groth, Juszkiewicz, & Ostriker 1989):

$$\xi_{\alpha\beta}(\mathbf{r}) \equiv \langle v_\alpha(\mathbf{r}')v_\beta(\mathbf{r}'+\mathbf{r})\rangle_{\mathbf{r}'}, \qquad (4.7)$$

where α and β denote spatial components of peculiar velocity $\mathbf{v}(\mathbf{r})$ of galaxies or clusters located at a position $\mathbf{r}$. If the peculiar velocity field is homogeneous and isotropic, the velocity correlation tensor can be expressed as (e.g., Monin & Yaglom 1975)

$$\xi_{\alpha\beta}(r) = [\Pi(r) - \Sigma(r)]\,\hat{r}_\alpha\hat{r}_\beta + \Sigma(r)\delta_{\alpha\beta}, \qquad (4.8)$$

where $\delta_{\alpha\beta}$ is the Kronecker delta and the hat denotes unit vector. Thus the tensor is characterized by the parallel and perpendicular components, $\Pi(r)$ and $\Sigma(r)$. Groth

et al.(1989) examined $\Pi(r)$ and $\Sigma(r)$ of galaxies in spiral and elliptical samples separately in the CMB frame which are plotted as symbols in Figures 8a to 8d. Velocity correlation tensors of galaxies and clusters derived in our simulations are shown in solid and dashed curves, respectively. We obtain the peculiar velocity of a cluster from simulations simply by computing its center-of-mass velocity from all particles grouped and assigned to the cluster by the ALM. We selected the clusters whose masses are greater than $1.2 \times 10^{13} M_{\odot}$ for SCDM and $4.2 \times 10^{12} M_{\odot}$ for LCDM. Their velocity correlation functions are basically the same as those of galaxies. This is due to the fact that the velocity dispersions of clusters are somewhat smaller than those of galaxies in our simulations.

As shown in Figure 8, both the SCDM and LCDM models exhibit considerably smaller amplitudes of the galactic velocity correlations than the observational estimates by Groth et al. (1989). The behavior of the SCDM model in linear regime is in good agreement with their result. Taken at face value, this poses a serious problem to both the SCDM and LCDM models. Since the number of sample galaxies (385 ellipticals and 201 spirals) is not large enough in a statistical sense, and the systematic bias (if any) in the distance indicator appreciably affects the estimate of the peculiar velocity, it might be premature to take the discrepancy so seriously at this point. The further observational study in this direction, of course, is of great importance.

5. DYNAMICAL PROPERTIES OF HALOS AND CLUSTERS IN SPATIALLY FLAT CDM UNIVERSE

In addition to the spatial distribution of galaxies and clusters, their dynamical properties also give us useful constraints about cosmological models. We here espatially pay attention to a velocity function (§5-1) and angular momenta (§5-2) in spatially flat CDM models. In addition to the present properties of galacies and clusters, we are also interested in the statistical distribution of proto-galactic objects (§5-3), because it would play a central role in developing the Hubble sequence of galaxies in the course of the subsequent dissipative evolution as well as the star formation rate. The CDM simulations which are used in this section are GS_{30}, GL_{40}, CS_{200} and CL_{300}, and the detail analysis in them is shown as follows.

5.1 Velocity Functions of Halos and Clusters

A velocity function (VF) is defined as the number density of objects as a function of their circular velocity V_c, in which it is important how to determine circular velocities of halos and clusters. Since the observed velocity function is estimated using either the HI line width or the stellar velocity dispersions, we computed VF by means of three different estimators: V_T, V_{max}, V_σ. The first estimator V_T uses the total mass and the maximum radius for each object. Since V_c varies with the radius r from the center of the object unless the density profile is in proportion to r^{-2}, we defined our second estimator V_{max} as the maximum value of $V_c(r)$ for each object. Finally we defined the third estimator V_σ using the one-dimensional velocity dispersion σ of the object as in Shimasaku (1993):

$$V_\sigma \equiv \sqrt{2}\sigma. \tag{5.1}$$

The resulting VF for halos and clusters from our simulations is plotted in Figure 9. A line represents the theoretical prediction of VF by means of the

Press-Schechter formalism whose detail expression is shown in Appendix A. In addition, the observational results by Shimasaku (1993) also exhibit. Note that our selection criterion $N_{mem} \geq 10$ leads to a systematic underestimate of the actual VF on small velocity regimes, $V_c \lesssim 100$km/s for halos and $V_c \lesssim 500$km/s for clusters. Apart from those regimes, the agreement of $n(V_T)$ and $n(V_{max})$ is quite good implying that the $\rho \propto r^{-2}$ profile approximates the objects selected in our simulations. In order to show the identification dependence clearly, we also examine $n(V_T)$ for different r_s, and confirm that our results do not be affected by the grouping method which we adopted here. It is found that our simulation in the SCDM models with $b = 1.7$ reproduces well VF on galaxy scales predicted in the PS theory, while the PS theory slightly underestimates VF from simulations on cluster scales ($V_c \gtrsim 1000$km/sec). On the other hand, the LCDM simulations produce VF with systematically lower amplitude compared with the PS theory while their slopes are quite similar. The same tendency with respect to the mass function was reported in Watanabe et al. (1993). Since equation (A.7) was originally derived in the Einstein-de Sitter ($\Omega_0 = 1$ and $\lambda_0 = 0$) universe, it would be reasonable that the SCDM models exhibit better agreement. Further critical comparison between simulations and the PS prediction, however, would not be meaningful, because it was shown that the overall factor in the PS function depends on the shape of the window function in defining the mass fluctuations. As a matter of fact, it is difficult to specify the window function in our ALM for particle grouping. Furthermore the departure from the spherically symmetric top-hat collapse assumed in the PS theory may be required in the LCDM models where the large-scale power is stronger than in the SCDM models. Therefore it is likely that VF computed using N-body simulations is more appropriate in confronting models with observations.

With the above remarks, we conclude that the observed VF for galaxies cannot be reconciled with the LCDM model prediction, and the discrepancy between the simulation and observation for galactic VF amounts to more than a factor of 10 around $V_c \sim 100$km/sec. Because this cannot be reconciled by changing the biasing

parameter b (Shimasaku 1993), it should be regarded as a serious difficulty for the LCDM model which has been one of the most successful scenarios so far (Ostriker & Suto 1990; Efstathiou et al. 1990; Suginohara & Suto 1992; Watanabe et al. 1993). The SCDM model, on the other hand, reproduces the amplitude and shape of the observed VF with the high bias $b_\rho \sim 2$; our result for $b = 1.7$ produces a slightly larger amplitude on cluster scales than observed, but with $b = 2.0$ the agreement would be improved (c.f., Shimasaku 1993). The high bias required for the SCDM model, however, is inconsistent with the COBE normalization (Smoot et al. 1992). In this respect, these constraints from VF as well as the spatial analysis in §4, all CDM models with the primordial Harrison–Zel'dovich spectrum would be in serious difficulty.

5.2 Spatial Distribution of Angular Momenta of Halos and Clusters

The statistic and spatial distribution of the angular momentum are closely related to its specific physical origin. So it is also important to examine the statistical distribution and the spatial correlation of angular momenta of halo and cluster. The dimensionless angular momentum λ[†] introduced by Peebles (1971) is a famous expression used to estimate the angular momentum of galaxies. The definition of the dimensionless angular momentum is

$$\lambda \equiv J|E|^{1/2}G^{-1}M^{-5/2} \tag{5.2}$$

where J, E, and M are the angular momentum, the total energy, and the total mass of the objects, and G is the gravitational constant. From the observational point of view, there exists few galaxies whose dimensionless angular momentum is more than 0.1 (Davis et.al.(1983), Gunn (1987)). This is one of important results

† According to the standard notation, we use λ_0 to indicate the dimensionless cosmological constant at the present epoch. This should not be confused with the dimensionless angular momentum λ which does not have the subscript 0.

to constrain cosmological models. In addition, there are several observational attempts to search for a possible signature of the spatial correlation of the angular momentum of galaxies, although it is quite difficult to perform a similar observational task for clusters of galaxies. For instance, Hawley and Peebles (1975) selected 5,559 galaxies in the areas which lie in Ursa Major, Coma, and Virgo cluster direction, and measured the direction of rotation axis. They did not find any apparent evidence of an anisotropy of the orientation of galaxies. Recently Iye & Sugai (1991) compiled a catalog of the spatial distribution of the angular momentum of 8,287 spiral galaxies from the ESO/Uppsala survey of the ESO (B) Atlas. They did not find any anisotropic distribution of the angular momentum orientation, either. Similar null result was also reported by Kashikawa & Okamura (1992). Therefore there seems no apparent anisotropy of the orientation of galaxies, and this is a second constraint of the cosmologycal models.

Now we estimate the dimensionless angular momentum λ in halos and clusters in our simulations with the same catalog of halos and clusters in the VF analysis, whose distribution function is shown in Figure 10. The histogram is plotted in a logarithmically equal bin $\Delta(\log\lambda) = 0.125$. The value of λ ranges rather broadly ($0.01 \lesssim \lambda \lesssim 0.1$), but there is a sharp cutoff around $\lambda \sim 0.2$. Since the distribution functions for all models look quite similar, the λ-distribution is quite insensitive to the underlying cosmology. Note that the different selection parameter r_s hardly changes the resulting distribution function. Mean values of λ (Table 4) are ~ 0.05 in all models. The mean value $\langle\lambda\rangle$ decreases very weakly as the total mass increases; histograms in dashed lines correspond to objects the number of whose member particles N_{mem} is ≥ 30 rather than ≥ 10. Anyway the SCDM and LCDM models do not contradict with the obserbational result.

Another interesting point to be checked is whether or not there is a significant correlation between λ and the local density, which have an important implication on the origin of the Hubble sequence. Figure 11 plots the cumulative probability function $P(>\lambda)$. Three different curves correspond to the different local density;

specifically galaxies are divided to three groups according to the radius R_5 centered at each galaxy and enclosing nearest other five galaxies. Although the effect is not too large, there is a clear tendency that halos with relatively large λ reside preferentially at low-density regions (i.e., large R_5). If the halos with large (small) λ are interpreted as spirals (ellipticals), this is consistent with the observational morphology-density relation (Postman & Geller 1984).

We next examined the spatial orientation of galaxies in SCDM and LCDM, and found that both models have no anisotropy. Therefore the CDM model does not contradict with the observational result. Moreover correlations between angular momenta of nearby galaxies were examined, and at present, it seems that observational studies have not yet reach any statistically significant conclusion on the spatial correlation of the angular momentum of galaxies. This is also consistent with our CDM model predictions; we were not able to detect any significant spatial correlation of angular momentum for our objects. Furthermore, we studied a possible distortion of the distribution of the angular momentum vectors for the nearest pair of objects. The angle θ in Figure 12 is defined by the angular momentum vectors of one object and its nearest neighbor (denoted by spin – spin), or by the relative position vector of the pair and the angular momentum vector of one of the pair (denoted by spin – position). As is clear in Figure 11, our results do not show any noticeable spatial correlation. We have also computed the angular momentum correlation tensor as a function of the pair-separation and found no feature in the tensor, either. Therefore no spatial correlation would be observed, provided that the angular momentum of the real galaxies is generated as in the present CDM models.

5.3 Evolution of Halos and Clusters

Before ending this section, we finally examine the evolution of halos and clusters. With the progress of recent photometric and spectroscopic observations, it would be possible to have statistically reliable samples of high redshift galaxies

and clusters in near future. Then it is of great value to prove the early cosmological evolution by means of analysing VF and angular momentum. In order to compute $n(V_T)$ at high z, we have applied our ALM independently to the data at each redshift and the results of evolution of VF are illustrated in Figure 13 together with the PS predictions. At high redshifts, the results of our simulations significantly deviate from the PS prediction which for the LCDM models, systematically overestimates VF of our simulations as in the case of $z = 0$. The more remarkable feature, however, is that the simulated VF hardly evolves even on cluster scales in the SCDM models, in marked contrast to the PS theory, and we think that further detailed study is needed to confirm this behavior. It is interesting to note, however, that Gunn (1990) reported an observational indication that the number density of rich clusters as large as Come at $z \sim 0.8$ is nearly equal to that in the present universe, i.e., the evolution of the cluster number density is very small. This indication, although not statistically reliable, disagrees with the PS prediction in SCDM models, but is quite consistent with our simulation results. The PS predictions suffer from two uncertainties after all, and direct analyses of numerical simulations are more relevant, or at least complementary, in comparing with observations.

Evolution of angular momentum of proto-galaxy was first to compute by Peebles (1969) on the basis of perturbation theory. He found that J in a spherical Eulerian volume grows only to second order, i.e., $J(t) \propto a(t)^2 D_1(t)\dot{D}_1(t)$, where $D_1(t)$ is the linear growth rate of density fluctuations. Later Doroshkevich (1970) pointed out that $J(t)$ computed in general configurations grow to first order, i.e., $J(t) \propto a(t)^2 \dot{D}_1(t)$. In the Einstein – de Sitter universe, the above growth rates reduce to $J(t) \propto a(t)^{3/2} \propto t$ (first order) and $J(t) \propto a(t)^{5/2} \propto t^{5/3}$ (second order). This behavior was confirmed by means of N-body simulations by White (1984) and Barnes & Efstathiou (1987). In Figure 14, we have plotted our result for 20 most massive objects in each model. It indicates that the first–order growth rate (dot-dashed lines) is consistent with $J(t)$ of each object at early epoch except for some

fluctuations which would be ascribed to merging with nearby clumps. In fact, the averaged angular momentum J over all halos and/or clusters (solid circles) shows better agreement with the first order growth. As is mentioned in previous works (e.g., Barnes & Efstathiou 1987), the angular momentum is mostly acquired in the linear stage, and the subsequent nonlinear evolution possibly including the mergers of clumps decreases the angular momentum. This is why the evolution of J for galactic objects deviates earlier and more significantly from the linear theory prediction than for clusters. Finally we plotted the evolution of distribution functions for λ at different redshifts in Figure 15. The shape of the distribution function seems almost the same, but the median value of the λ shifts towards larger values as z increases.

6. SUMMARY AND DISCUSSION

The principal aim of the present paper is to obtain some predictions about the value of density parameter by means of analysing the spatial and dynamical properties of galaxies and clusters properly identified in cosmological N-body simulations. For identifying groups of particles in simulation data we applied the ALM algorithm. For definiteness, we considered two spatially flat CDM models with $\Omega_0 = 1.0,\ \lambda_0 = 0.0\ b_\rho = 1.7$ (SCDM) and $\Omega_0 = 0.2,\ \lambda_0 = 0.0\ b_\rho = 1.0$ (LCDM). Main conclusions are as in the following;

We have attempted to find an alternative measure to characterize the pattern of galaxy clustering other than the two-point correlation function. Various statistical measures based on either counts-in-cells or the multifractal approach are successful to some extent, but none seems to be particularly superior to the two-point correlation function in discriminating the underlying structure. The average dimensionality obscures the various different structures. While the relation between

f_{occ} and f_{per} reflects the complementary feature of the pattern to that revealed by the two-point correlation function, it is significantly affected by the sampling condition of the data. All of the models from the simulations exhibit a multi-fractal nature, though the dependence on the cell size ϵ is stronger than that on the intrinsic pattern in each model. This would be inevitable in some sense, since due to the discrete nature of the galaxy distribution, multi-fractal measures are defined only in a somewhat ambiguous manner. It should be remarked that the two-point correlation fucntion is only the second moment of the distribution averaged over the direction, and ,thus, might not necessarily contain all of the statistical properties of the distribution. Although this is quite true, the observed distribution of galaxies are well described in the framework of the hierachical clustering models by means of the two-point correlation function (e.g., Balian and Schaeffer 1988,1989; Fry 1984; Vogeley et al. 1991;Gaztañaga and Yokoyama 1992); the two-point correlation function is basically the single quantity to represent the statistical distribution.

The shape of two-point spatial correlation functions of clusters is similar to those of galaxies within the statistical uncertainties in both models, but their correlation lengthes are sensitive both to the specific value of Ω_0 and to the sizes of the clusters (or their number density). As in earlier studies (e.g., White et al. 1987), the SCDM model has not been able to explain the correlation length as large as observed (c.f., Bahcall 1988). Clusters in the LCDM model, on the other hand, exhibit stronger correlations, and reproduce remarkably well the observed empirical relation between the correlation length and the mean separation of clusters. Velocity correlation functions of galaxies in either SCDM or LCDM models behave quite differently from those estimated observationally by Groth et al. (1989). This requires further careful examinations both theoretically and observationally. The shape of VF for halos and clusters in our simulations is in good agreement with that predicted in the PS theory, while the overall amplitude is consistent within a factor of two. The best agreement is obtained on galactic scales 100 km/sec $\lesssim V_c \lesssim$ 600 km/sec in SCDM model, while the LCDM models generally lead to systematically

smaller $n(V_c)$ compared with the PS prediction. These results support the earlier conclusion by Shimasaku (1993) that the observed VF is not consistent with CDM model predictions except SCDM with $b \sim 2$ which, however, is in conflict with the COBE result (Smoot et al. 1992). While more statistically reliable determination of VF of galaxies and clusters is necessary, this seems to rule out almost all CDM models with the Harrison–Zel'dovich primordial spectrum. The distribution of the dimensionless angular momentum λ is very broad, $0.01 \lesssim \lambda \lesssim 0.1$, as was known previously. We found for the first time that the functional form of the distribution looks very universal and are quite insensitive both to the cosmological parameters and to the fluctuation spectrum shape. The spatial distribution of angular momenta of halos and clusters does not show noticeable correlation of the orientation either in SCDM or in LCDM model. Galaxies with relatively small λ preferentially cluster around dense regions, which would be closely related to, and likely to be consistent with, the observed morphology-density relation of galaxies (Postman & Geller 1984). The evolution of the angular momentum in early epochs is consistent with the perturbation theory proposed by Doroshkevich (1970). We have confirmed that it grows to first order also in LCDM models.

It should be noted that VF for clusters of galaxies is closely related to their X-ray temperature function. In fact, Suginohara (1993) found that observed temperature function prefers a high bias SCDM $b \sim 2$ using his smoothed particle hydrodynamic simulations, which is consistent with our finding with respect to VF of galaxies and clusters. Apparently this would pose one serious problem to the LCDM model which has been one of the most successful scenarios so far (Ostriker & Suto 1990; Efstathiou et al. 1991; Suginohara & Suto 1992; Watanabe et al. 1993). It is an important problem to examine how J and λ are redistributed in disks in the course of the dissipative and hydrodynamic evolution of galaxies. Apparently this is beyond the scope of the present paper and SPH (smoothed particle mesh) simulations will gives us some informations about this question.

ACKNOWLEDGMENTS

It is a pleasure to thank Y. Suto who invite us at this topic and give many useful suggestions and comments. Thanks are also due to M. Itoh, T. Suginohara, K. Shimasaku, S. Sawada, A. Ishikawa for their helpful discussions. We would like to acknowledge a careful reading of the manuscript by K. Tomita. We want to express our gratitude to other members of Yukawa Institute of Uji research center for their warmly encouragements.

APPENDIX A

We here exibit the derivation of a theoretical expression for the VF on the basis of the PS mass function (Press & Schechter 1974; White & Frenk 1991):

$$n(M,z)dM = -\left(\frac{2}{\pi}\right)^{1/2}\frac{\rho_0}{M}\frac{\delta_c}{\Delta^2(M,z)}\frac{d\Delta(M,z)}{dM}\exp\left[-\frac{\delta_c^2}{2\Delta^2(M,z)}\right]\,dM. \quad \text{(A.1)}$$

In the above, the mass function $n(M,z)$ indicates a comoving number density of objects of mass in the range of M and $M+dM$ at a redshift z, ρ_0 is the present mass density in the universe, δ_c is the *linear* density contrast of objects at the (top-hat) collapse epoch (Peebles 1980; Lilje 1992), and $\Delta(M,z)$ is the density fluctuation smoothed over a mass scale of M at the redshift z. Using linear theory, the last quantity is computed by

$$\Delta^2(M,z) = \frac{D_1^2(z)}{2\pi^2}\int_0^\infty P_0(k)W^2(kr_0)\;k^2dk, \quad \text{(A.2)}$$

where $D_1(z)$ is the linear growth rate (e.g., Peebles 1980), $P_0(k)$ is the power-spectrum of density fluctuations at the present epoch ($z=0$), and $W(kr_0)$ is the window function for the comoving length r_0 corresponding to the mass scale M:

$$W(kr_0) = \frac{3}{k^3r_0^3}(\sin kr_0 - kr_0\cos kr_0) \qquad r_0 \equiv \left(\frac{3M}{4\pi\rho_0}\right)^{1/3}. \quad \text{(A.3)}$$

The above top-hat window function is most appropriate in the PS theory, but the overall normalization factor varies depending on the specific choice (see, Bond et al. 1991).

Let us rewrite the mass function (A.1) in terms of the the circular velocity $V_c(M)$ of objects of mass M and radius R:

$$V_c \equiv \sqrt{\frac{GM}{R}}. \quad \text{(A.4)}$$

If we assume that the radius R of objects is given as the half of the turnaround radius $r_{ta}(M,z)$ of the dissipationless spherical collapse, one may relate R with the

corresponding comoving radius $r_0 = r_0(M)$. In the Einstein – de Sitter universe, for instance, the density $\rho_{vir}(z)$ of clumps which virialize at a redshift z is given by $18\pi^2$ times the background density at that epoch $\bar{\rho}(z)$ independently of the mass M (e.g., Peebles 1980, §19). Following Shimasaku (1993), we define the collapsing factor δ_{max}:

$$\delta_{max}(z) \equiv \frac{r_0(M)}{r_{ta}(M,z)}. \tag{A.5}$$

Then equation (A.4) for objects virialized at z with mass M is rewritten as

$$V_c(M,z) = \sqrt{\frac{GM}{0.5 r_{ta}(M,z)}} = H_0 \Omega_0^{1/2} \delta_{max}^{1/6}(z) r_0(M). \tag{A.6}$$

Then equation (A.1) reduces to

$$\begin{aligned} n(V_c,z)dV_c = -\frac{3}{(2\pi)^{3/2}} \delta_c H_0^2 \Omega_0 \delta_{max}^{1/3} \times \\ \frac{1}{\Delta^2(M,z)} \frac{1}{V_c^3} \frac{d\Delta(M,z)}{dr_0} \exp\left[-\frac{\delta_c^2}{2\Delta^2(M,z)}\right] dV_c. \end{aligned} \tag{A.7}$$

This is the VF predicted in the PS theory. In arbitrary Ω_0 and λ_0, the collapse factor $\delta_{max}(z)$ for objects at a redshift z has to be numerically integrated on the basis of the spherical nonlinear model (see Figure 3 of Shimasaku 1993). In practice, however, the following approximate formula (White, Efstathiou, & Frenk 1993) proved to show good agreement with his numerical results for $\Omega_0 < 1$ models which we consider here:

$$\delta_{max}(z) = \frac{\rho_{vir}(z)}{8\bar{\rho}(z=0)} \sim \frac{9\pi^2}{4} \frac{(1+z)^3}{\Omega(z)^{0.6}} \tag{A.8}$$

$$\Omega(z) \equiv \frac{\Omega_0}{\Omega_0 - (\Omega_0 + \lambda_0 - 1)(1+z)^{-1} + \lambda_0 (1+z)^{-3}} \tag{A.9}$$

Therefore we used the above formula in computing the VF (A.6) with the CDM power-spectrum given by Davis et al. (1985) as the present spectrum $P_0(k)$ whose

normalization is fixed by $(\delta M/M)(8h^{-1}\mathrm{Mpc}) = 1/b$. We set $\delta_c = 3(12\pi)^{2/3}/20 \sim 1.69$ throughout (Lilje 1992).

REFERENCES

Bahcall, N.A. 1979, *ApJ*, **232**, 689.

Bahcall, N.A. 1988, *ARA&A*, **26**, 631.

Bahcall, N.A., & Soneira, R.M. 1983, *ApJ*, **270**, 20.

Bahcall, N.A., & West, M. 1992, *ApJ*, **392**, 419.

Balian, R. and Schaeffer, R. 1989, *Astron.Astrophys.*, **220**, 1.

Bond, J. R., Cole, S., Efstathiou, G., & Kaiser, N. 1991, *ApJ*, **379**, 440.

Dalton, G.B. Efstathiou,G. Maddox, S.J. & Sutherand, W.J. 1992, *ApJ*, **390**, L1.

Davis, M., Efstathiou, G., Fall, S.M., Illingworth, G. & Schechter, P. 1983, *ApJ*, **266**, 41.

Davis, M., Efstathiou, G., Frenk, C.S., & White, S.D.M. 1985, *ApJ*, **292**, 371.

Davis,M. & Peebles,P.J.E. 1983, *ApJ*, **267**, 465.

de Lapparent, V., Geller, M.J., and Huchra, J.P. 1989, *Astrophys.J.*, **343**, 1, (dLGH).

Dressler,A., Faber, S.M., Burstein, D., Davies, R.L., Lynden-Bell, D., Terlevich, R.J. & Wegner, G.1987, *ApJ*, **313**, L37.

Efstathiou,G., Sutherland, W.J., & Maddox, S.J. 1990, *Nature*, **348**, 705.

Fry, J.N. 1984, *Astrophys.J.Letters*, **277**, L5.

Gaztañaga, E., and Yokoyama, J. 1993, *ApJ*, **403**, 450.

Górski, K., Davis, M., Strauss, M.A., White, S.D.M. & Yahil, A. 1989, *ApJ*, **344**, 1.

Groth, E.J. Juszkiewicz, R. & Ostriker, J.P. 1989, *ApJ*, **346**, 558.

Gunn, J.E. 1987, in *The Galaxy*, eds. by Gilmore & Carswell, (Reidel),413.

Guth,A.H. 1981, *Phys.Rev.*, **D23**, 347.

Hernquist, L., Bouchet, F. R., & Suto, Y. 1991, *ApJS*, **75**, 231.

Harrison, E.R. 1970, *Phys.Rev.*, **D1**, 2726.

Itoh, M. 1990, *Publ. Astron. Soc. Japan.*, **42**, 481.

Jones, B.J.T., Martinez, V.J., Saar, E., and Einasto, J. 1988, *Astrophys.J.Letters*, **332**, L1.

Kaiser, N. 1987, *MNRAS*, **227**, 1.

Lilje. 1992, *ApJ*, **386**, L33.

Maddox, S.J., Efstathiou, G., Sutherland, W.J., & Loveday, J. 1990, *MNRAS*, **242**, 43p.

Martinez, V.J., Jones, B.J.T., Dominguez-Tenreiro, R., and van de Weygaert, R. 1990, *Astrophys.J.*, **357**, 50.

Monin, A.S., & Yaglom, A.M. 1975, *Statistical Fluid Mechanics, Vol. 2* (MIT Press Cambridge).

Nichol, R.C. Collins, C.A. Guzzo, L. & Lumsden, L. 1992, *MNRAS*, **223**, 21p.

Ostriker, J.P. & Suto, Y. 1990, *ApJ*, **348**, 378.

Peebles, P.J.E. 1971, *A&A*, **11**, 377.

Peebles,P.J.E. 1980, *The Large Scale Structure of the Universe* (Princeton University Press, Princeton).

Postman, M., & Geller, M.J. 1984, *ApJ*, **281**, 95.

Press, W.H. & Schechter, P. 1974, *ApJ*, **187**, 425.

Shimasaku, K. 1993, *ApJ*, **413**, 59.

Smoot,G.F., Bennett,C.L., Kogut,A., Wright,E.L., Aymon,J., Boggess,N.W., Cheng,E.S., DeAmici,G.,
Gulkis,S., Hauser,M.G., Hinshaw,G., Lineweaver,C., Loewenstein,K., Jackson,P.D., Janssen,M.,
Kaita,E., Kelsall,T., Keegstra,P., Lubin,P., Mather,J.C., Meyer,S.S., Moseley,S.H., Murdock,T.L., Rokke,L., Silverberg,R.F., Tenorio,L., Weiss, R. & Wilkinson,D.T. 1992, ApJ, submitted.

Strauss, M., Cen, R.Y., & Ostriker, J.P. 1992, ApJ, submitted.

Suginohara, T. 1993, PASJ, submitted.

Suginohara, T. & Suto, Y. 1992, *ApJ*, **399**, 395.

Suginohara, T. and Suto, Y. 1991b, *Publ.Astron.Soc.Japan.*, **43**, L1.

Suginohara, T. , Suto, Y., Bouchet, F.R., & Hernquist, L. 1991, *ApJS*, **75**, 631.

Suto, Y., Cen, R.Y., & Ostriker, J.P. 1992, *ApJ*, **394** , August 10 issue, in press.

Suto, Y., Gouda, N., & Sugiyama, N. 1990, *ApJS*, **74**, 665.

Suto, Y. & Suginohara, T. 1991, *ApJ*, **370**, L15.

Totsuji, H. & Kihara, T. 1969, *Publ.Astron.Soc.Japan.*, **21**, 221.

Ueda, H. 1993, PASJ, submitted.

Ueda, H., Itoh, M., & Suto, Y. 1993, *Publ.Astron.Soc.Japan.*, **45**, 7.

Ueda, H., Itoh, M., & Suto, Y. 1993, *ApJ*, **408**, 3.

Ueda, H., Shimasaku, K., Suginohara, T., & Suto, Y. 1993, PASJ, submitted.

Vogeley, M.S., Geller, M.J., and Huchra, J.P. 1991, *Astrophys.J.*, **382**, 44.

Watanabe, T., Matsubara, T., & Suto, Y. 1993, ApJ, submitted.

White, S.D.M., Efstathiou, G, & Frenk, C.S. 1993, *MNRAS*, **262**, 10.

White, S.D.M. & Frenk, C.S. 1991, *ApJ*, **379**, 52.

White, S.D.M., Frenk, C.S., Davis, M.,& Efstathiou, G., 1987 , *ApJ*, **313**, 505.

Wright,E.L., Meyer,S.S., Bennett,C.L., Boggess,N.W., Cheng,E.S., Hauser,M.G., Kogut, A., Lineweaver,C., Mather,J.C., Smoot,G.F., Weiss,R., Gulkis, S., Hinshaw,G., Janssen,M., Kelsall,T., Lubin,P.M., Moseley,Jr., S.H., Murdock,T.L., Shafer,R.A., Silverberg,R.F. & Wilkinson, D.T. 1992, ApJ, submitted.

Table 1. Simulation Parameters

model	Ω_0	λ_0	h	b_ρ	L_b	m_p	N_{obj}
$n=1$	1.0	0.0	1.0	1.0	—	—	262,144
$n=0$	1.0	0.0	1.0	1.0	—	—	262,144
$n=-1$	1.0	0.0	1.0	1.0	—	—	262,144
$n=-2$	1.0	0.0	1.0	1.0	—	—	262,144
GS_{30}	1.0	0.0	0.5	1.7	$30h^{-1}$Mpc	$7.1 \times 10^9 M_\odot$	6,291
GL_{40}	0.2	0.8	0.75	1.0	$40h^{-1}$Mpc	$2.3 \times 10^9 M_\odot$	3,913
GL_{100}	0.2	0.8	1.0	1.0	$100h^{-1}$Mpc	$2.1 \times 10^{11} M_\odot$	262,144
CS_{130}	1.0	0.0	0.5	1.7	$130h^{-1}$Mpc	$5.8 \times 10^{11} M_\odot$	8976
CS_{200}	1.0	0.0	0.5	1.7	$200h^{-1}$Mpc	$2.1 \times 10^{11} M_\odot$	16,229
CL_{100}	0.2	0.8	1.0	1.0	$100h^{-1}$Mpc	$2.1 \times 10^{11} M_\odot$	1404
CL_{300}	0.2	0.8	0.75	1.0	$300h^{-1}$Mpc	$9.5 \times 10^{11} M_\odot$	13,278

Table 2. Summary of measures quantifying galaxy clustering

model		$n=1$	$n=0$	$n=-1$	$n=-2$	GL_{100}
γ [a]	...	-2.8	-2.7	-2.1	-1.9	-1.9
r_0/L [b]	...	0.018	0.047	0.036	0.10	0.057
K [c]	...	4.5	8.8	3.1	2.8	2.3
β [c]	...	0.9	1.0	1.1	1.2	1.2
F [d]	...	0.097	0.076	0.067	0.056	0.054
D_0 [e]	...	2.4(1.8)	2.3(1.8)	2.5(1.8)	2.5(1.8)	2.5(1.8)
D_1 [e]	...	2.2(1.8)	2.0(1.7)	2.3(1.8)	2.3(1.8)	2.3(1.8)
D_2 [e]	...	2.1(1.7)	1.8(1.6)	2.0(1.8)	1.9(1.8)	2.0(1.8)
D_{10} [e]	...	1.8(1.5)	1.4(1.4)	1.6(1.6)	1.3(1.5)	1.5(1.5)

[a] spectral indices of two-point correlation functions fitted to a single power-law $\propto r^{\gamma}$ at $\xi(r)=1$.

[b] correlation lengths where $\xi(r_0)=1$.

[c] fitted in the range of $n_{exp} \leq 1.0$.

[d] filling factor.

[e] fractal dimensions for $\epsilon = 1/100$. The numbers in parentheses correspond to those for $\epsilon = 1/1000$.

Table 3. Slopes and correlation lengths of correlation functions

model	system		Mass ($M_\odot$)	γ	$r_0(h^{-1}\mathrm{Mpc})$
CS_{130}	galaxy	···	5.8×10^{11}	-2.0±0.1	2.6±0.1
	1.7σ peak	···	5.8×10^{11}	-1.9±0.03	4.4±0.2
	large cluster	···	$> 7.4 \times 10^{13}$	-2.3±0.2	4.7±1.3
	intermediate cluster	···	$> 2.9 \times 10^{13}$	-2.0±0.03	3.9±0.2
	small cluster	···	$> 1.2 \times 10^{13}$	-1.8±0.1	3.2±0.2
CL_{100}	galaxy	···	2.1×10^{11}	-1.8±0.1	5.1±0.5
	large cluster	···	$> 2.7 \times 10^{13}$	-2.1±0.1	11.6±2.6
	intermediate cluster	···	$> 1.1 \times 10^{13}$	-1.5±0.1	8.6±2.2
	small cluster	···	$> 4.2 \times 10^{12}$	-1.5±0.1	6.6±1.0

Table 4. Mean values of the dimensionless angular momentum of halos of galaxies

r_s/L_b	N_{mem}	GS_{30}	GL_{40}	CS_{200}	CL_{300}
1/128	≥ 10	0.06 ± 0.03	0.05 ± 0.03	0.05 ± 0.02	0.05 ± 0.03
1/128	≥ 30	0.04 ± 0.02	0.04 ± 0.02	0.04 ± 0.02	0.04 ± 0.02
1/64	≥ 10	0.05 ± 0.03	0.05 ± 0.03	0.05 ± 0.02	0.06 ± 0.03

Figure Captions

Figure 1: Particle projection on the x-y plane within the interval $-0.05 \leq z/L \leq 0.05$. a) $n = 1$ power law (A), b) $n = 0$ power law (B), c) $n = -1$ power law (C), d) $n = -2$ power law (D), e) GL_{100} (E).

Figure 2: Two-point correlation functions for models A $\sim$ E.

Figure 3: $(n_{exp}, n_{occ} - 1)$ relation for models A $\sim$ E.

Figure 4: $f_{occ} - f_{per}$ relation for models A $\sim$ E.

Figure 5: Generalized dimension D_q for models A $\sim$ E. a) $\epsilon = 1/100$, b) $\epsilon = 1/500$, c) $\epsilon = 1/1000$.

Figure 6: Two-point spatial correlation functions of galaxies and clusters of galaxies. a) CS_{130} in real space; b) CL_{100} (E) in real space; c) CS_{130} in redshift space; d) CL_{100} in redshift space.

Figure 7: Correlation lengths of clusters of galaxies plotted against the mean separations of clusters in the samples. The dotted lines are fits to the simulation results (filled squares for CL_{100} and filled circles for CS_{130}. Open symbols represent the correlation lengths of the simulation particles.

Figure 8: Peculiar velocity correlation functions of galaxies and clusters of galaxies. Also plotted are the observational estimates for elliptical and spiral galaxies (Groth et al. 1989) in the CMB frame. a) Parallel component $\Pi(r)$ in CS_{130}; b) Perpendicular component $\Sigma(r)$ in CS_{130}; c) Parallel component $\Pi(r)$ in CL_{100}; d) Perpendicular component $\Sigma(r)$ in CL_{100}.

Figure 9: Velocity function for halos and clusters. Open circles, open squares, and crosses indicate the results for the three estimators for the circular velocity V_c, i.e., V_T, V_σ and V_{max}, respectively. The prediction in the Press-Schechter theory is plotted in solid curves. The observational data (filled triangles) are taken from Shimasaku (1993). Both galactic and cluster scale simulation results are plotted in the same panel, (a) SCM (GS_{30} and CS_{200} models); (b) LCDM (GL_{40} and CL_{300} models).

Figure 10: Histograms for the dimensionless angular momentum λ. Solid and dashes lines

indicate distribution for $N_{mem} \geq 10$ and ≥ 30, respectively with $r_s = L_b/128$, while dot–dashed lines, $N_{mem} \geq 10$ with $r_s = L_b/64$. (a) GS_{30} , (b) GL_{40} , (c) CS_{200} , and (d) CL_{300} models.

Figure 11: Cumulative probability distribution function λ of halos. The objects are identified with $r_s = L_b/64$ and $\beta = 0.25$. They are divided to the three different groups according to the radius R_5 defined in the text; solid curves for $0 < R_5 < 0.6h^{-1}$Mpc, dashed curves for $0.6h^{-1}$Mpc $< R_5 < 1h^{-1}$Mpc, and dot-dashed curved for $R_5 > 1h^{-1}$Mpc.

Figure 12: Spatial distribution of the angular momentum. The number of nearest neighbor objects are plotted against $\cos\theta$, where θ is the angle between the angular momentum vectors of the nearest pairs (solid lines) or between the relative position vector and the angular momentum vector (dashed lines).

Figure 13: Evolution of velocity functions $n(V_T)$. Open symbols denote the simulation results while solid curves, the Press-Schechter predictions. (a) GS_{30} , (b) GL_{40} , (c) CS_{200} , and (d) CL_{300} models.

Figure 14: Evolution of J. The time evolution of J for 20 most massive objects identified at $z = 0$ in each simulation is plotted in solid lines. The filled circles indicate the average over all identified objects. Growth rate based on perturbation theory is plotted in dash – dotted lines (the amplitude is arbitrary).

Figure 15: Evolution of distribution of λ. The objects are identified with $r_s = L_b/64$ and $\beta = 0.25$ at each epoch.

Figure 1a

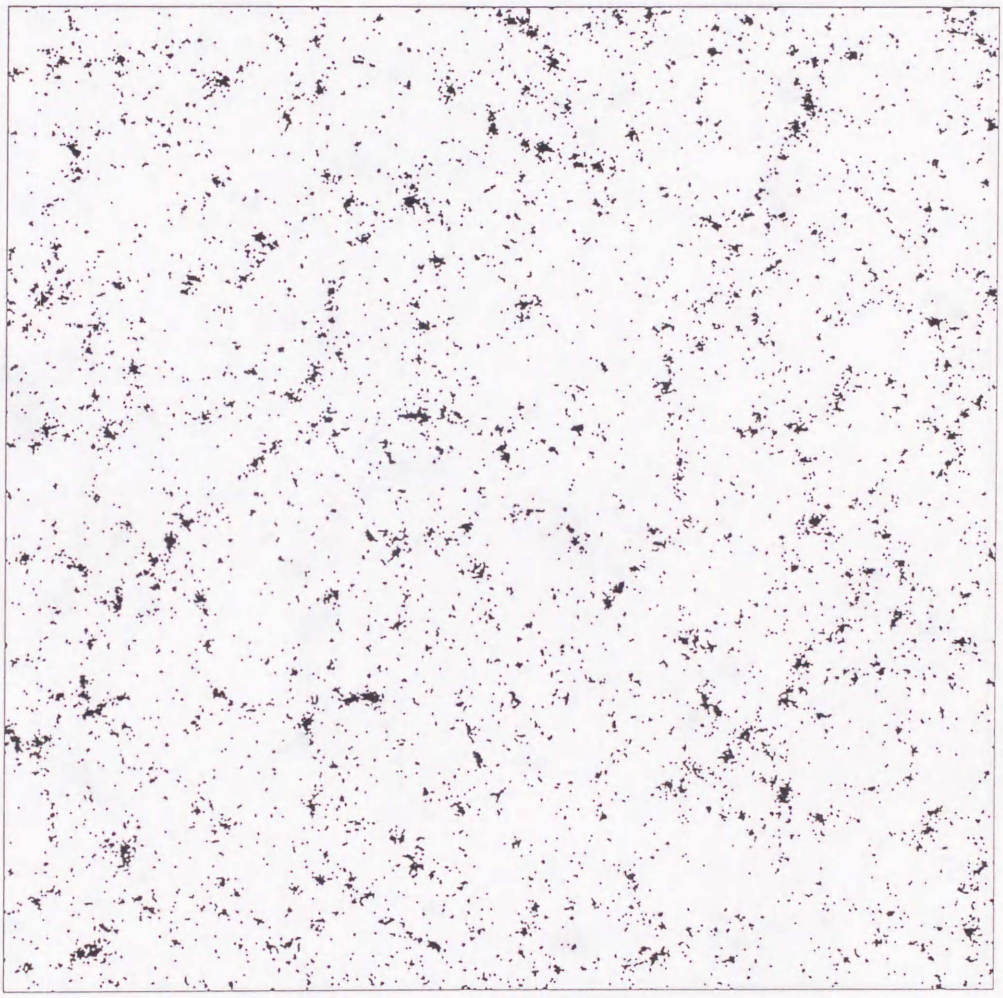

Data Name : power-law model n=1
Ω = 1.0
λ = 0.0
a/a_i = 18.21
Range of z : $-0.05 < z < 0.05$
Number of particles = 27489

Figure 1b

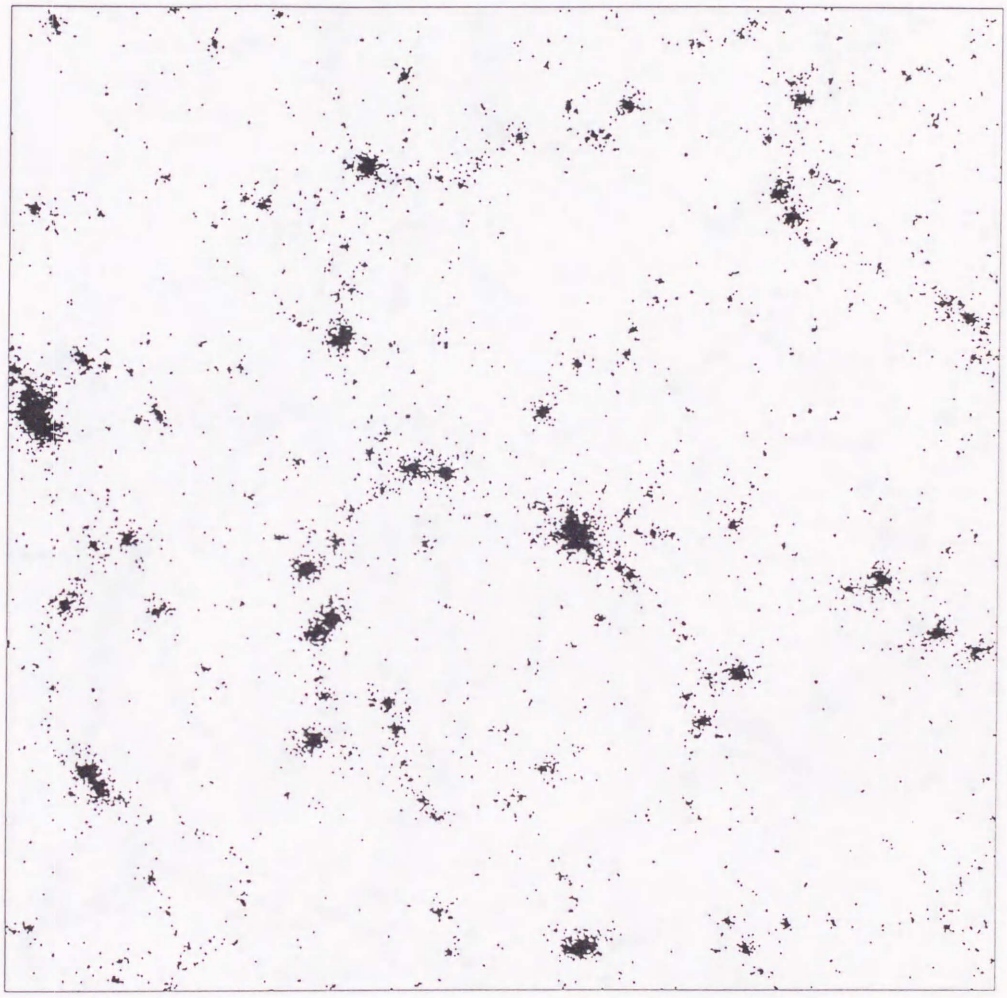

Data Name : power-law model n=0
Ω = 1.0
λ = 0.0
a/a_i = 37.60
Range of z : $-0.05 < z < 0.05$
Number of particles = 25948

Figure 1c

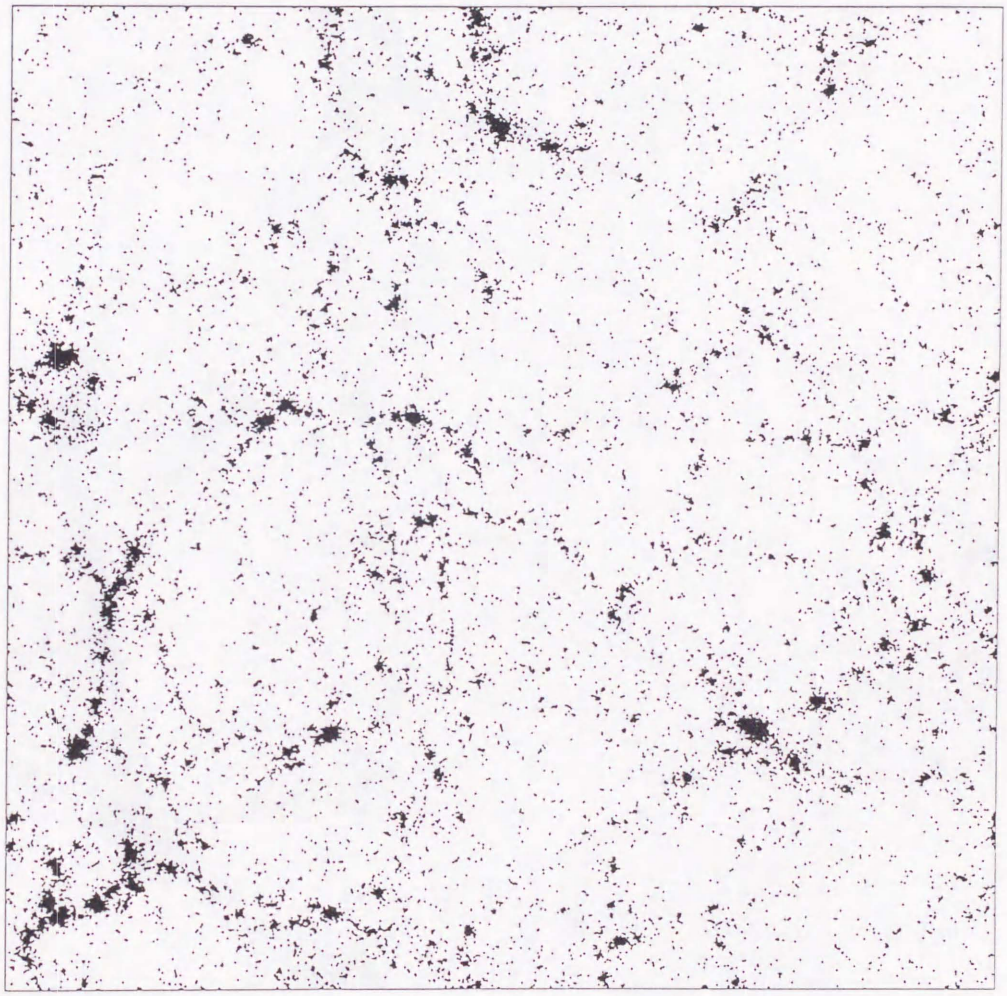

Data Name : power-law model n=-1
Ω = 1.0
λ = 0.0
a/a_i = 6.91
Range of z : $-0.05 < z < 0.05$
Number of particles = 28740

Figure 1d

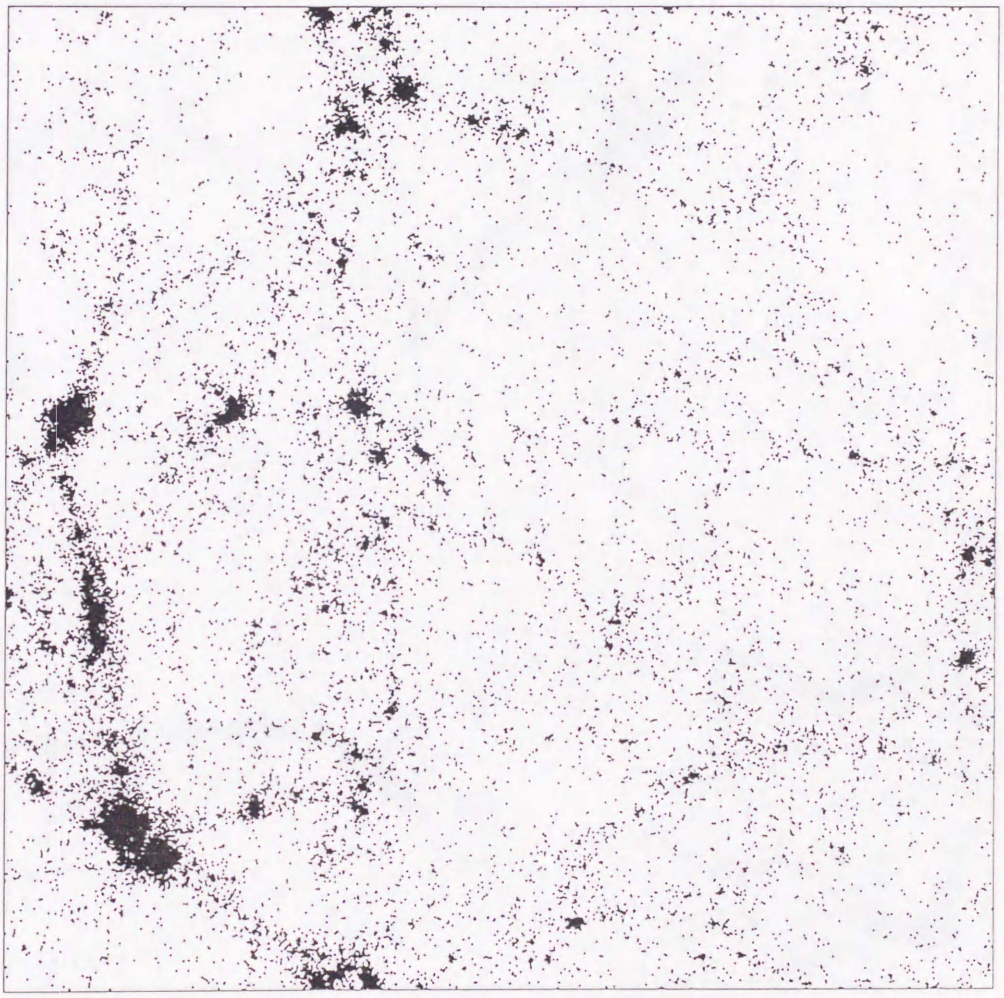

Data Name : power-law model n=-2
Ω = 1.0
λ = 0.0
a/a_i = 6.70
Range of z : $-0.05 < z < 0.05$
Number of particles = 32288

Figure 1e

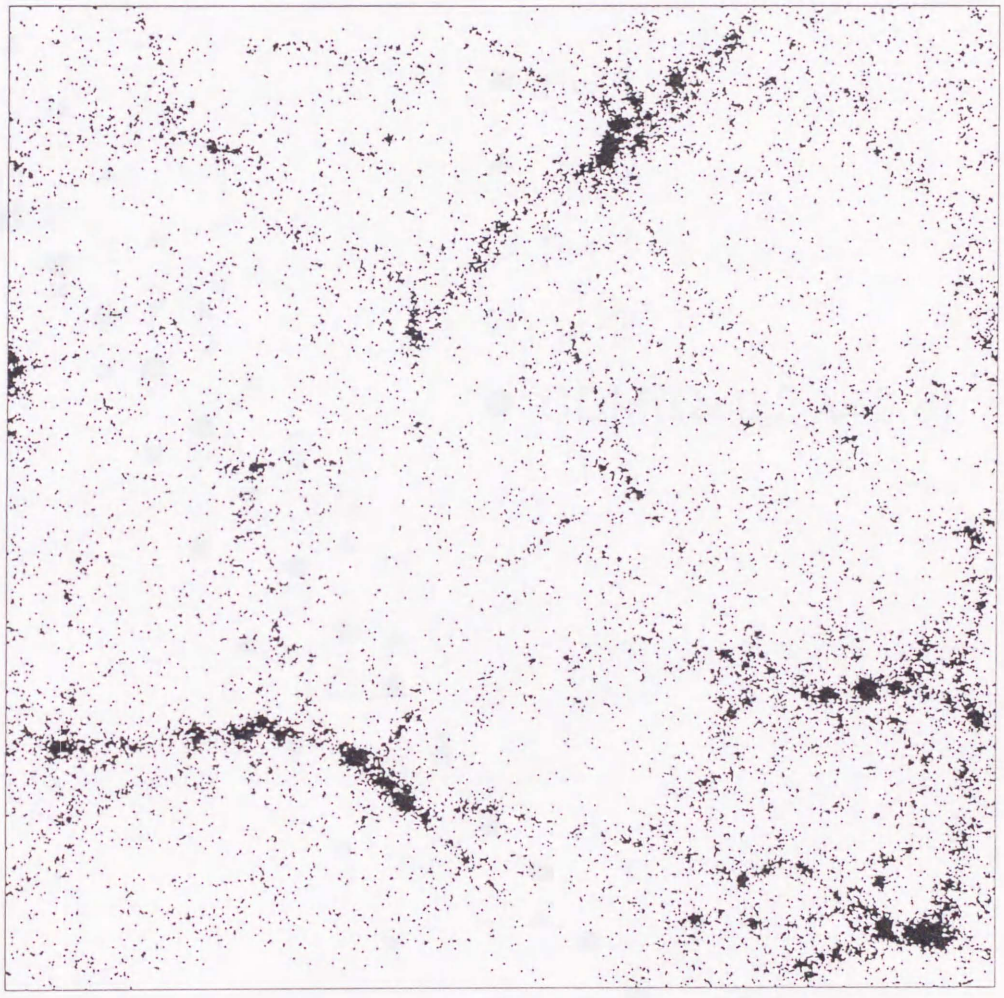

Data Name : CDM model
Ω = 0.2
λ = 0.8
a/a_i = 6.00
Range of z : $-0.05 < z < 0.05$
Number of particles = 28546

Figure 2

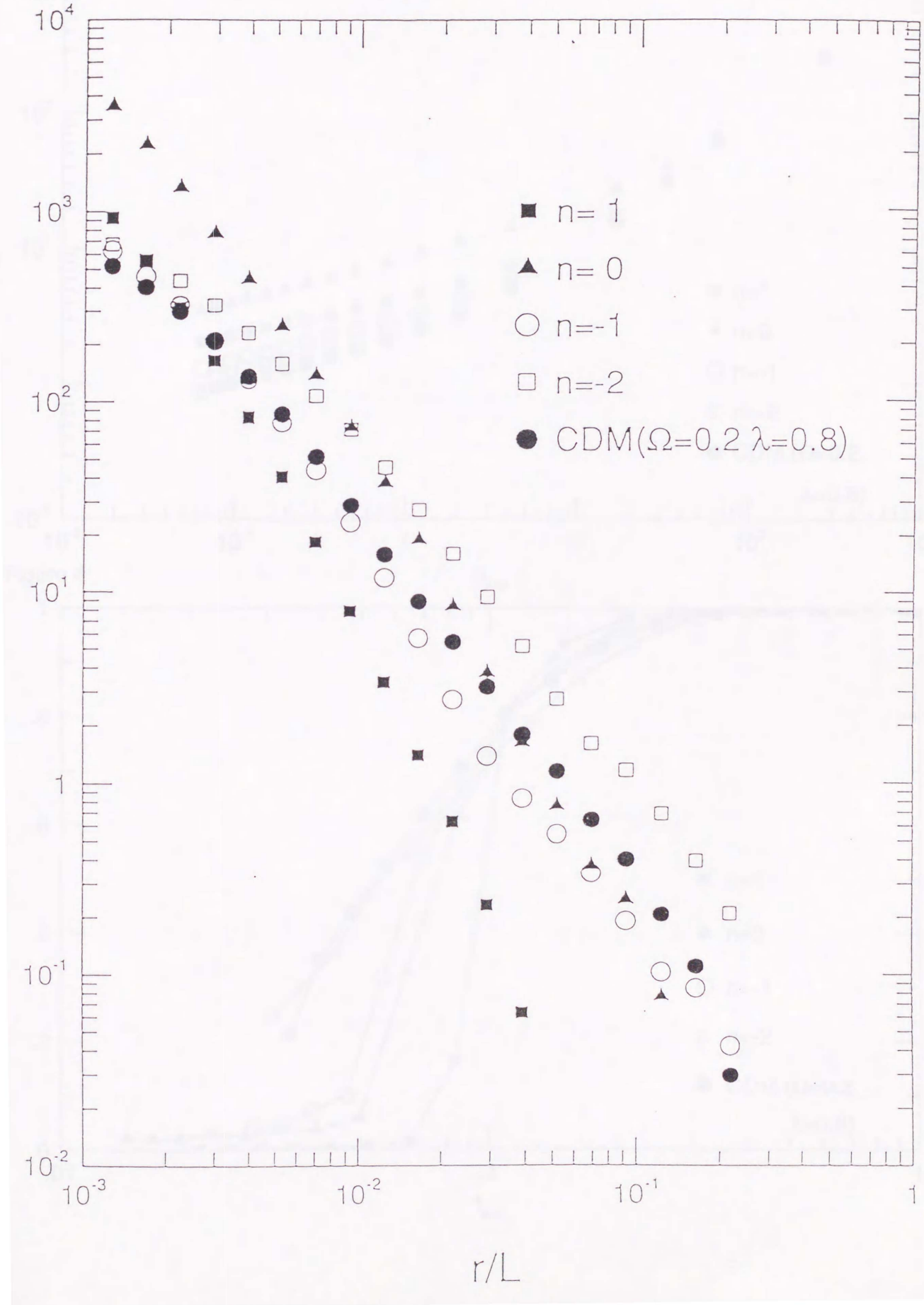

Figure 3

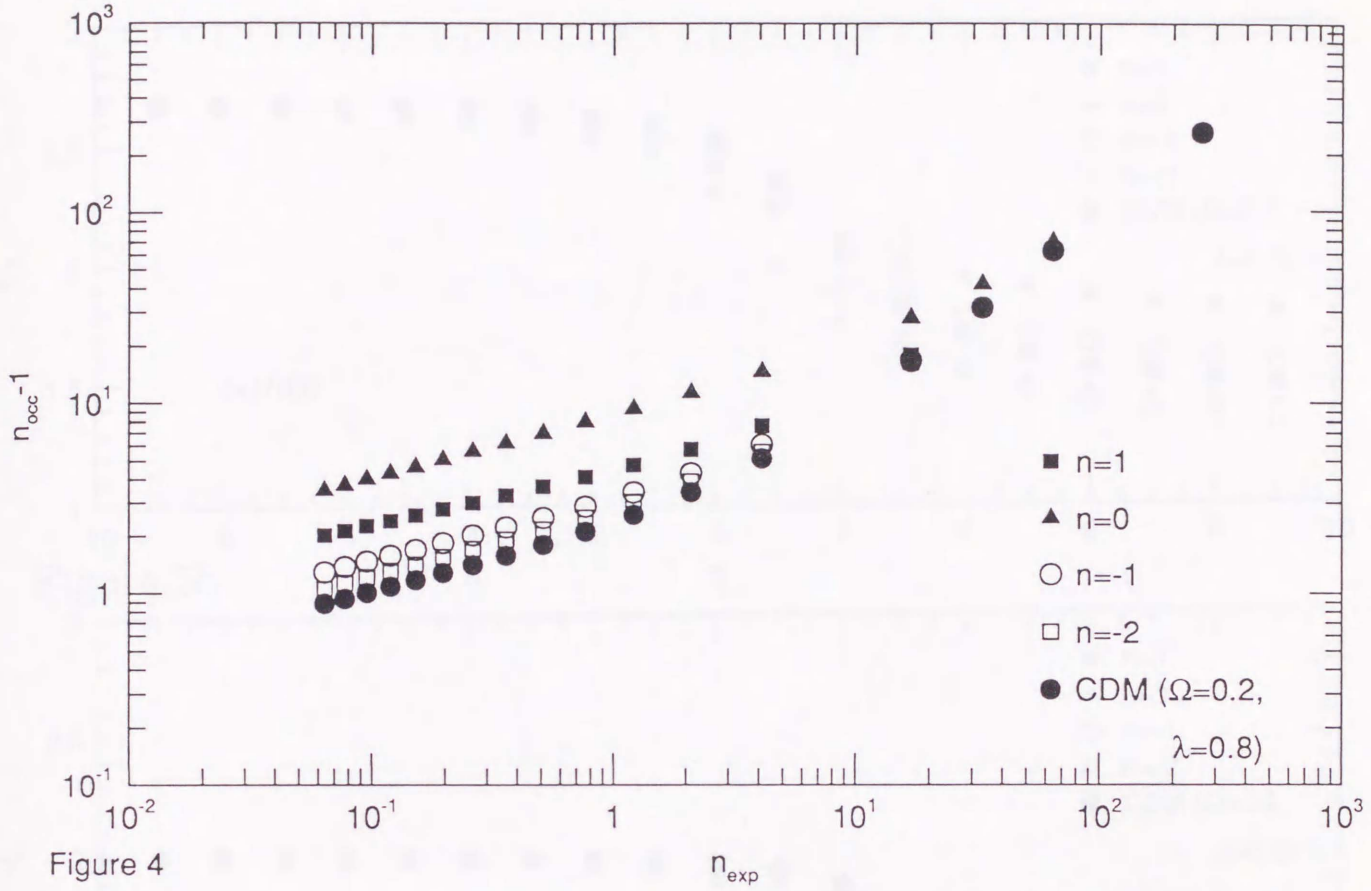

Figure 4

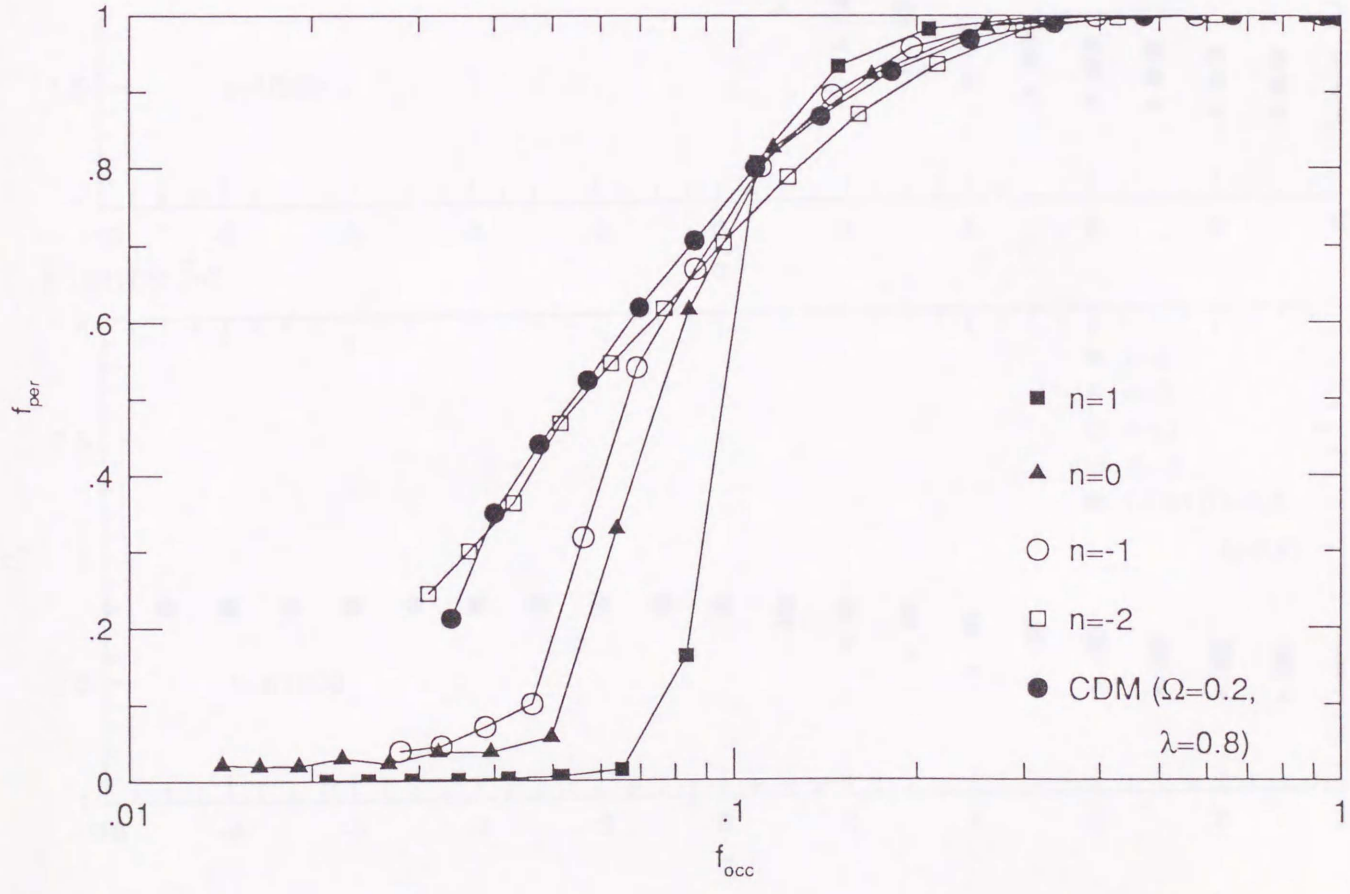

Figure 5a

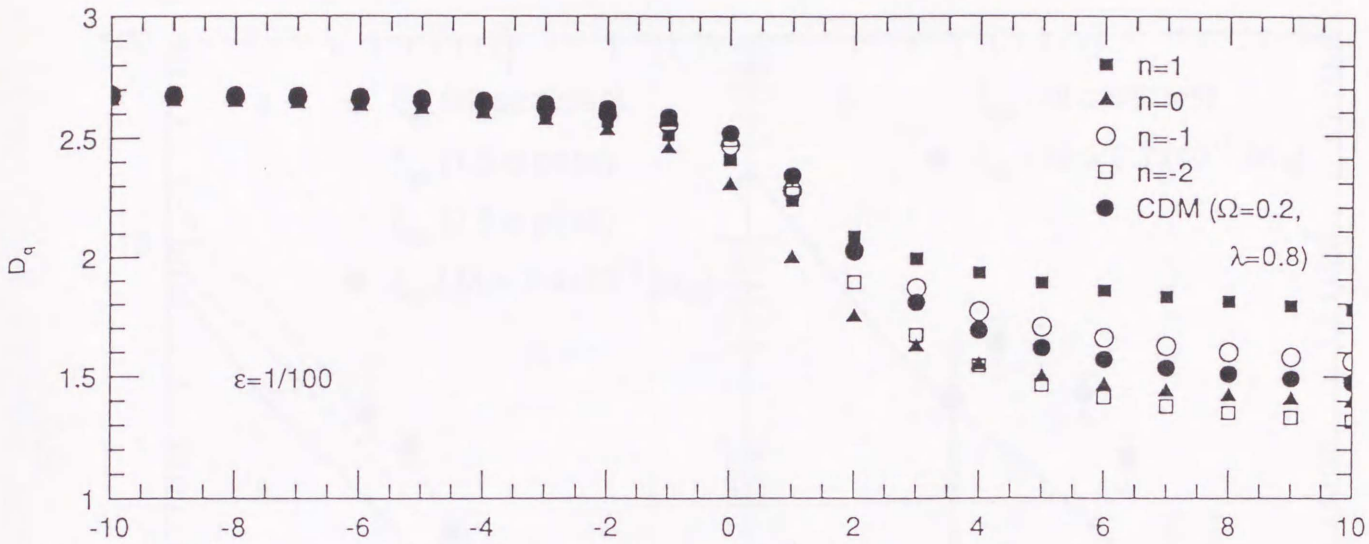

Figure 5b

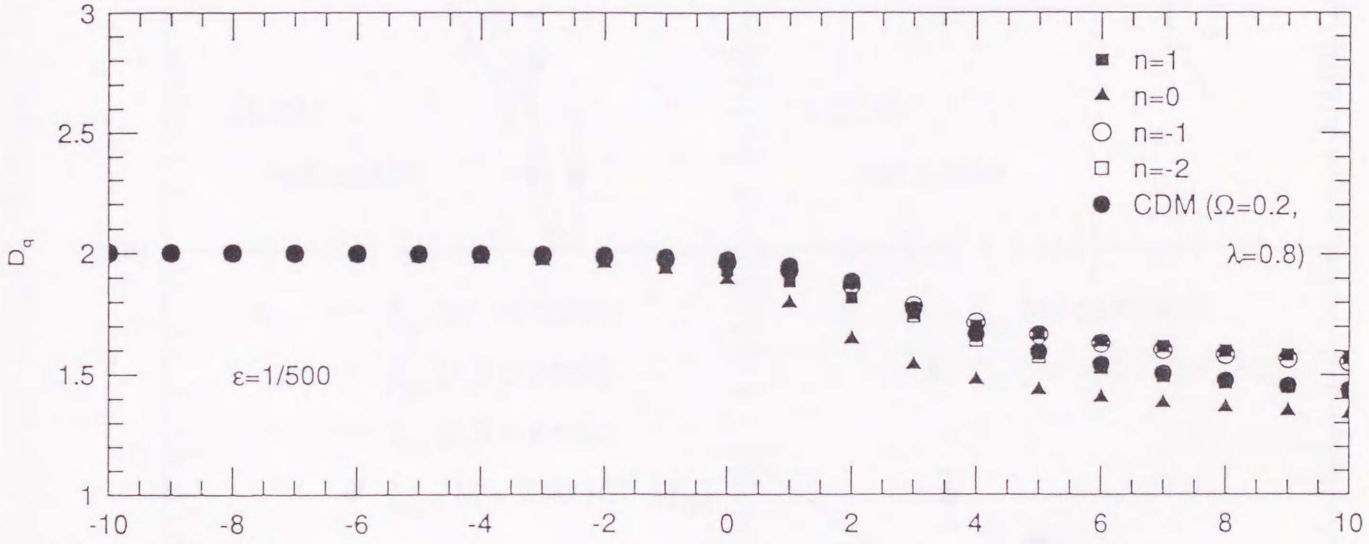

Figure 5c

Figure 6

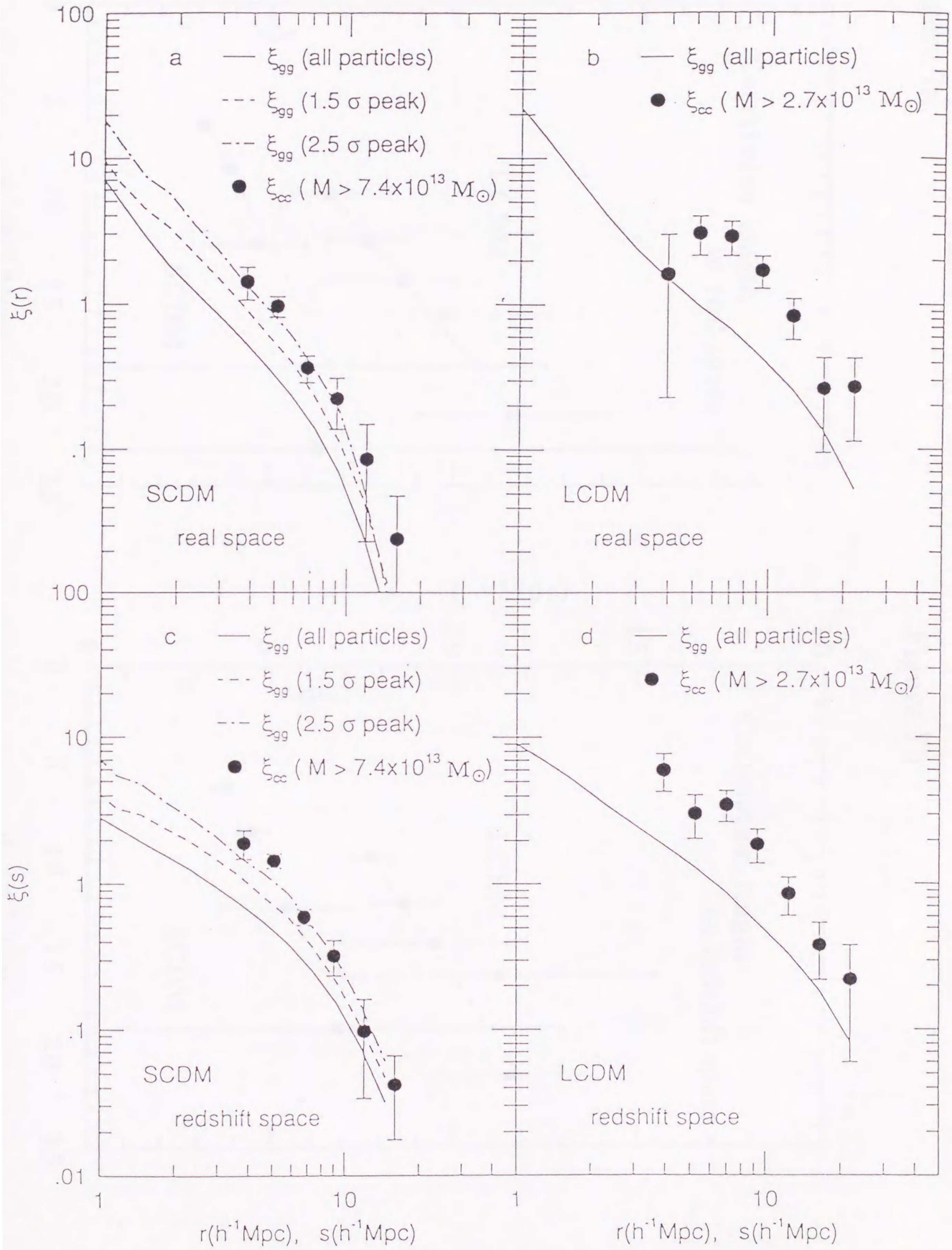
a
ξ_{gg} (all particles)
ξ_{gg} (1.5 σ peak)
ξ_{gg} (2.5 σ peak)
ξ_{cc} (M > 7.4x10^{13} M$_\odot$)
SCDM
real space
b
ξ_{gg} (all particles)
ξ_{cc} (M > 2.7x10^{13} M$_\odot$)
LCDM
real space
c
ξ_{gg} (all particles)
ξ_{gg} (1.5 σ peak)
ξ_{gg} (2.5 σ peak)
ξ_{cc} (M > 7.4x10^{13} M$_\odot$)
SCDM
redshift space
d
ξ_{gg} (all particles)
ξ_{cc} (M > 2.7x10^{13} M$_\odot$)
LCDM
redshift space
ξ(r)
ξ(s)
100
10
1
.1
.01
1
10
r(h^{-1}Mpc), s(h^{-1}Mpc)

Figure 7a

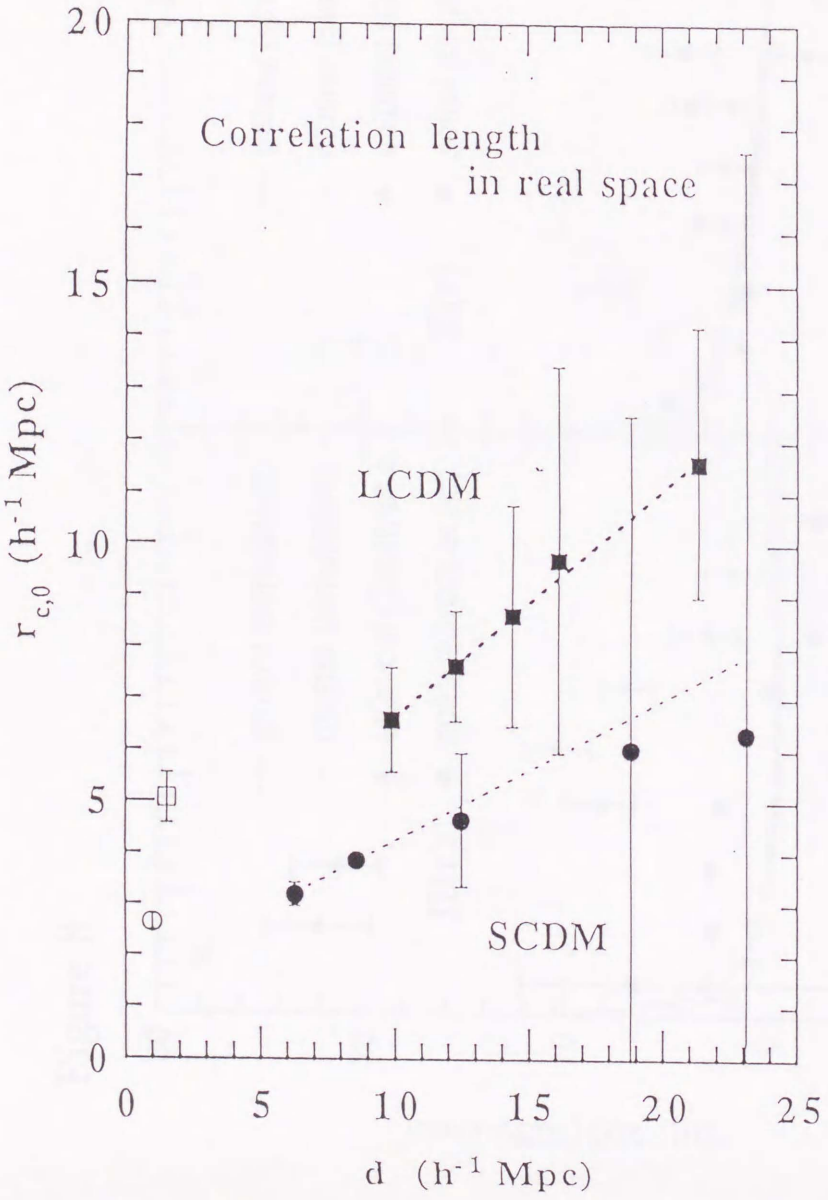

Figure 7b

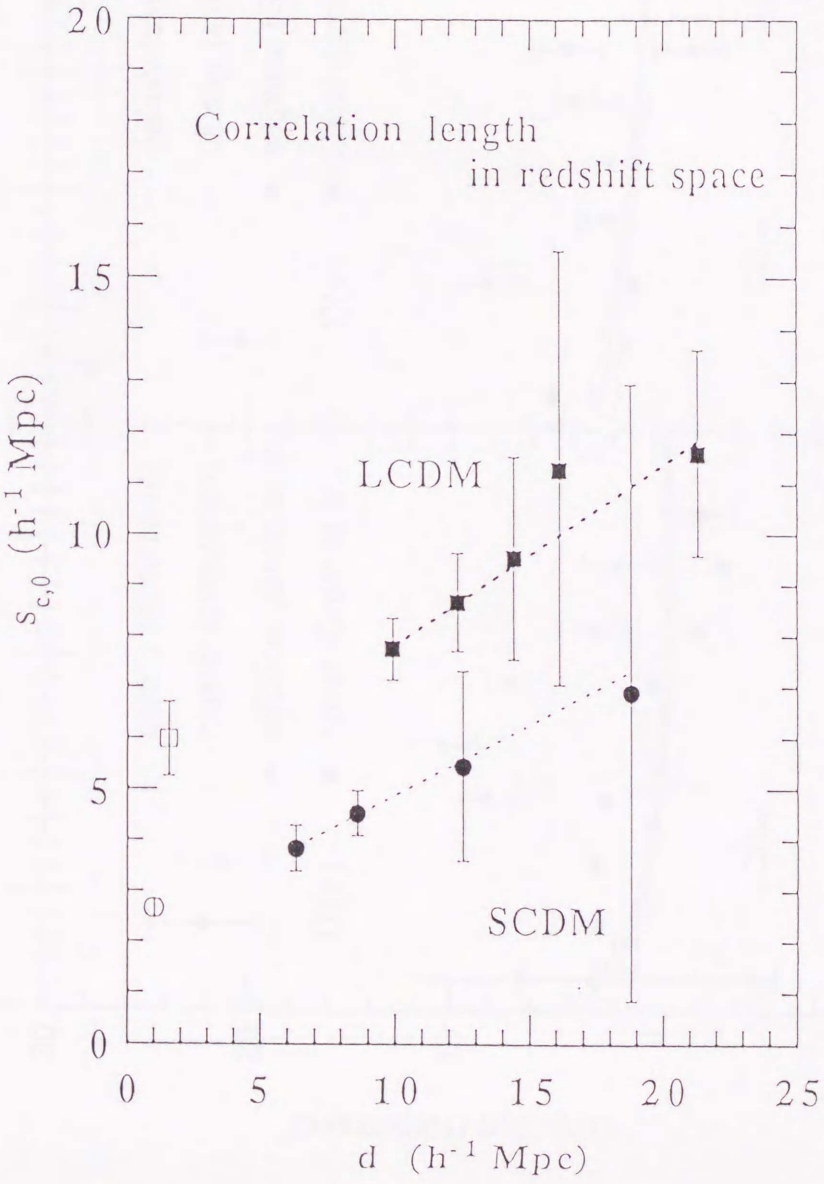

Figure 8

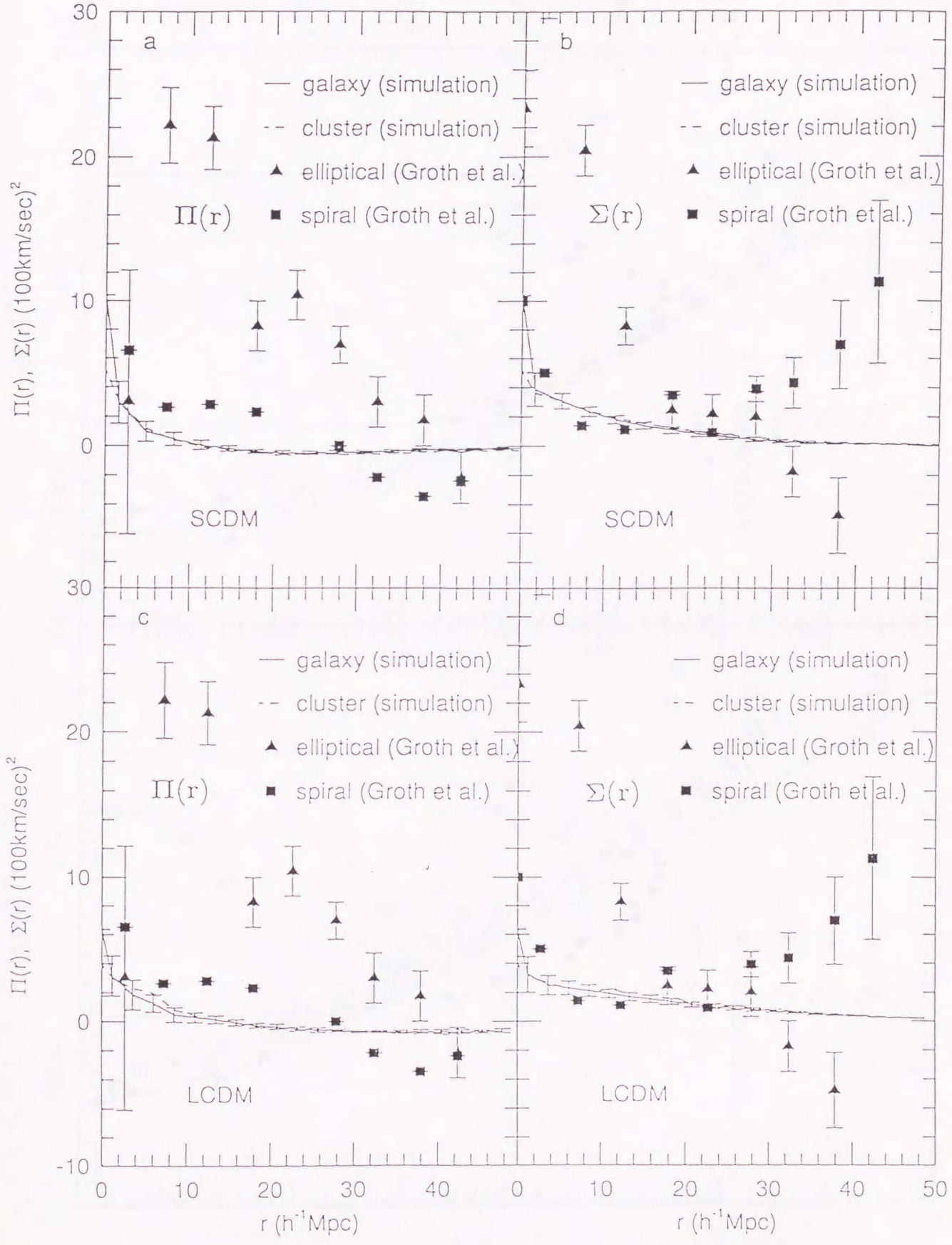
a
b
c
d
galaxy (simulation)
cluster (simulation)
elliptical (Groth et al.)
spiral (Groth et al.)
Π(r)
Σ(r)
SCDM
LCDM
Π(r), Σ(r) (100km/sec)²
r (h⁻¹Mpc)
30
20
10
0
-10
0
10
20
30
40
50

Figure 9

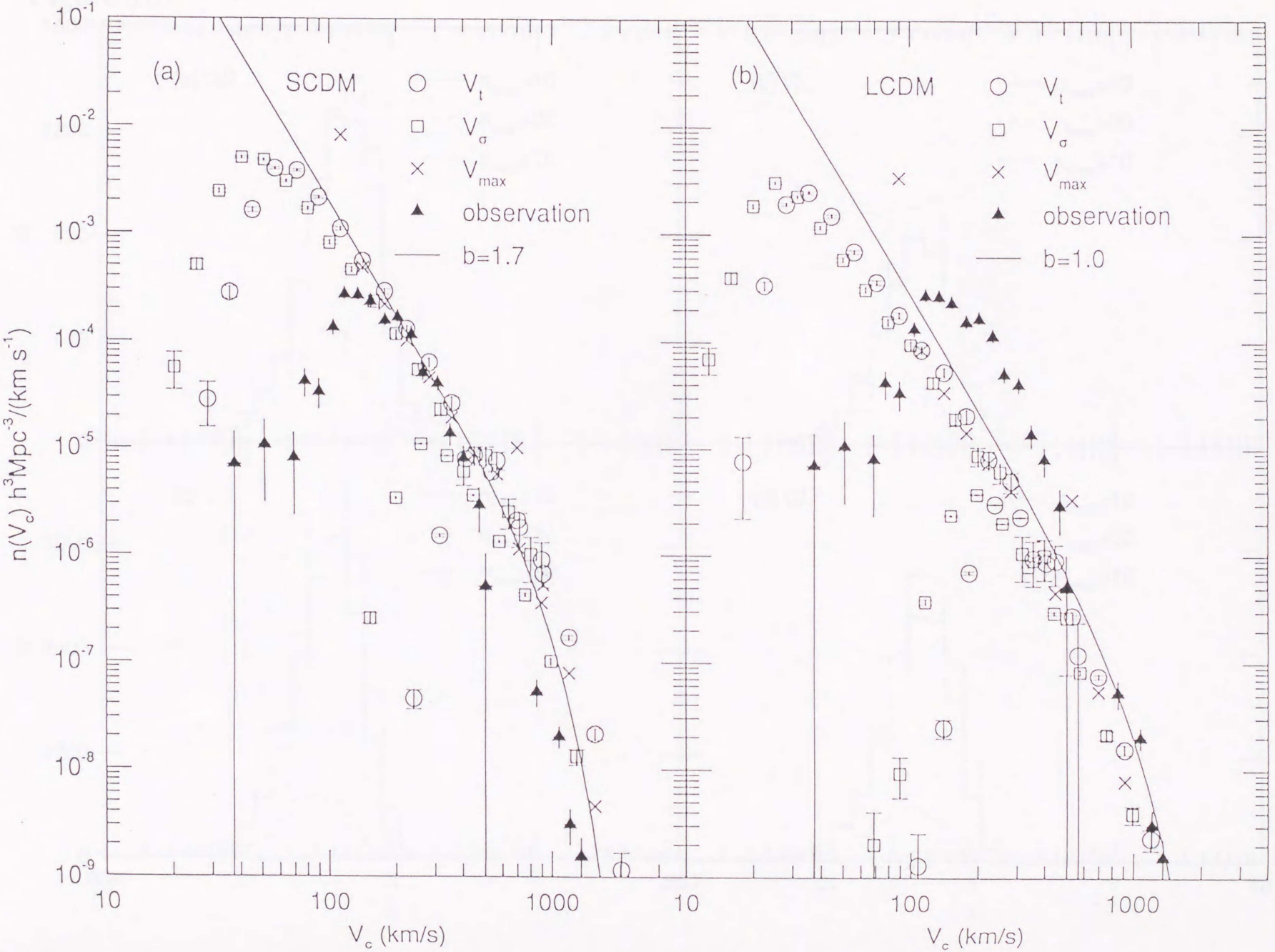
(a)
SCDM
V_t
V_σ
V_{max}
observation
b=1.7
(b)
LCDM
V_t
V_σ
V_{max}
observation
b=1.0
$n(V_c)\ h^3Mpc^{-3}/(km\ s^{-1})$
10^{-1}
10^{-2}
10^{-3}
10^{-4}
10^{-5}
10^{-6}
10^{-7}
10^{-8}
10^{-9}
10
100
1000
V_c (km/s)

Figure 10

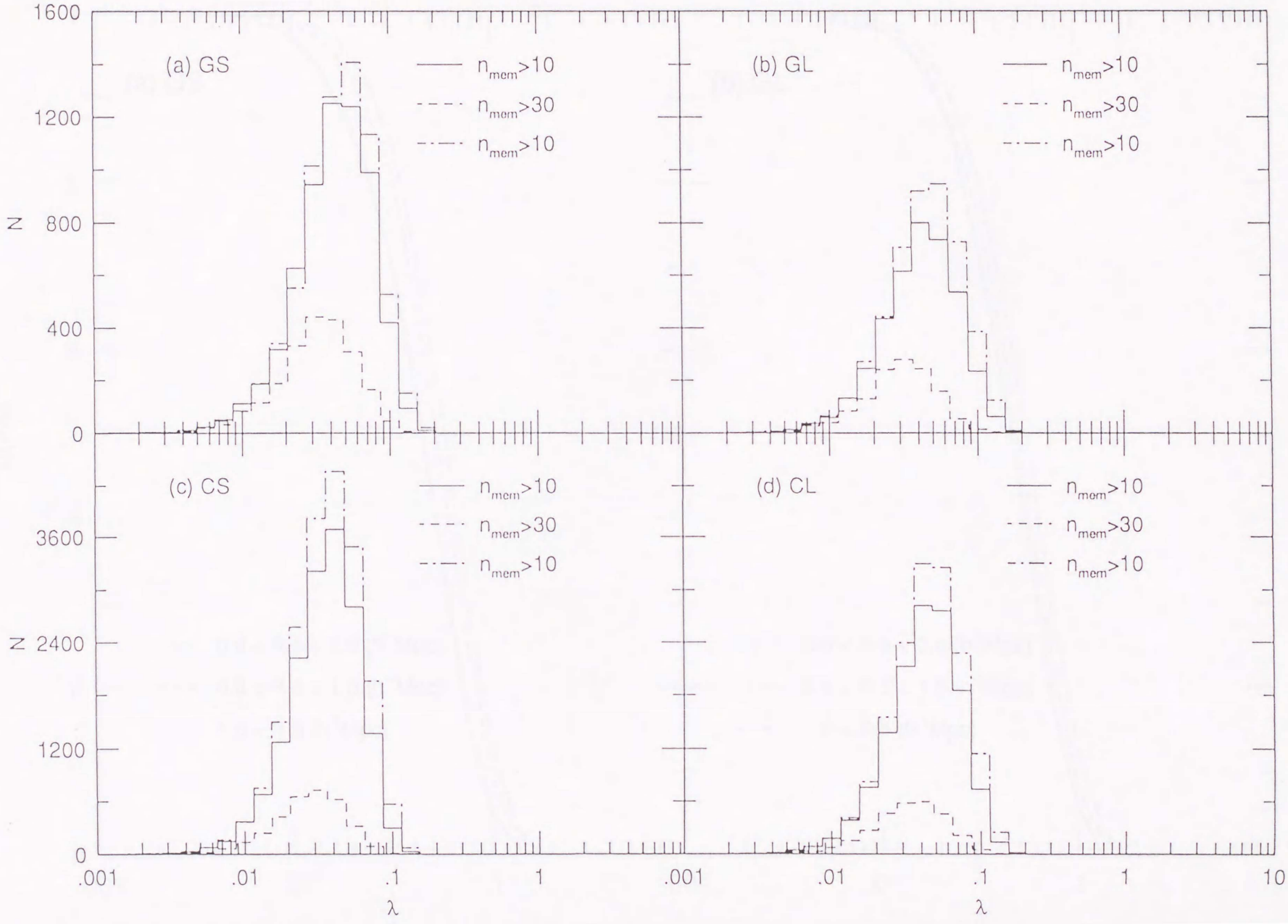
(a) GS
(b) GL
(c) CS
(d) CL
n_{mem}>10
n_{mem}>30
n_{mem}>10
N
λ
1600
1200
800
400
0
3600
2400
1200
.001
.01
.1
1
10

Figure 11

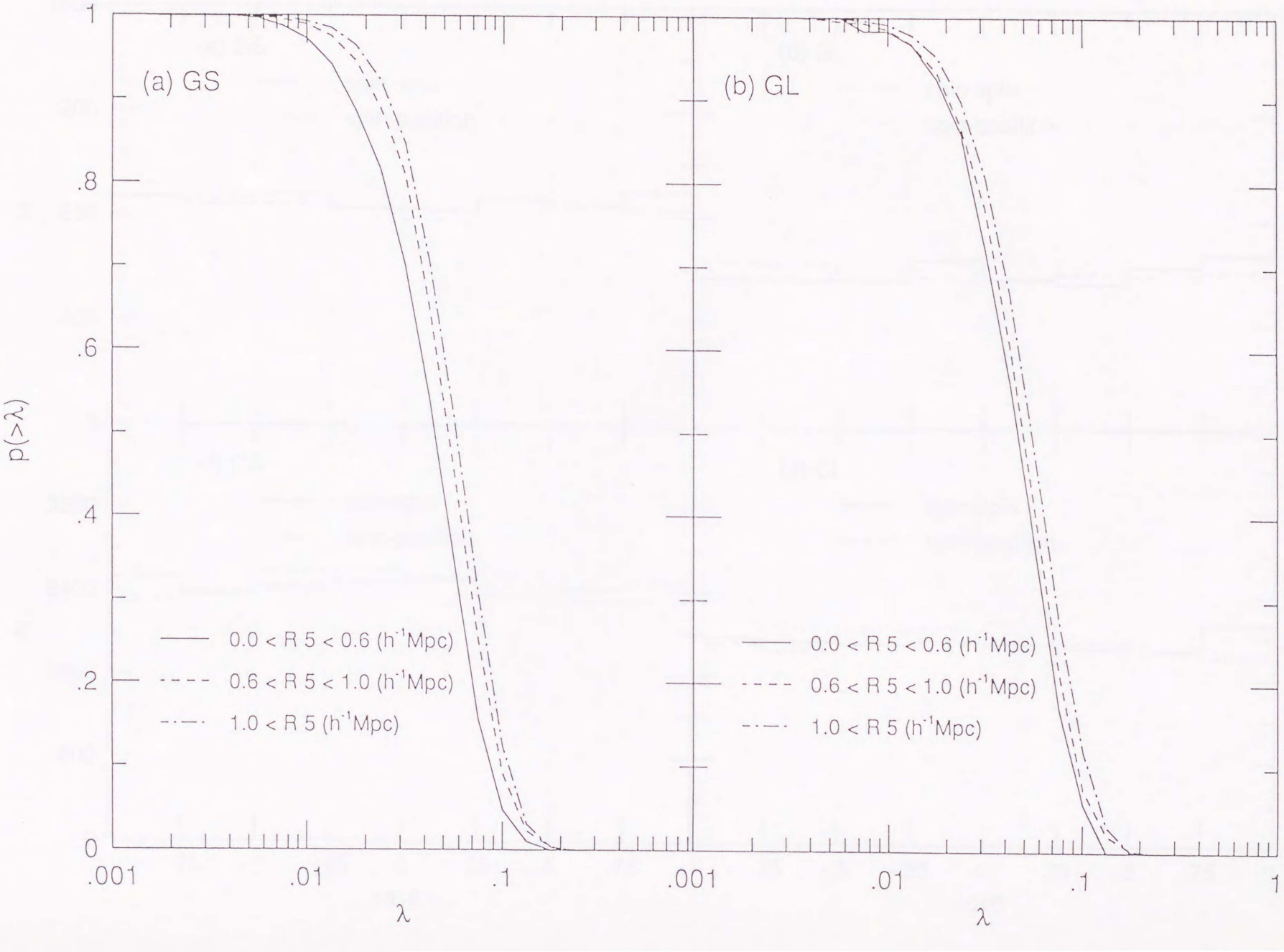
(a) GS
(b) GL
p(>λ)
λ
1
.8
.6
.4
.2
0
.001
.01
.1
1
0.0 < R 5 < 0.6 (h⁻¹Mpc)
0.6 < R 5 < 1.0 (h⁻¹Mpc)
1.0 < R 5 (h⁻¹Mpc)

Figure 12

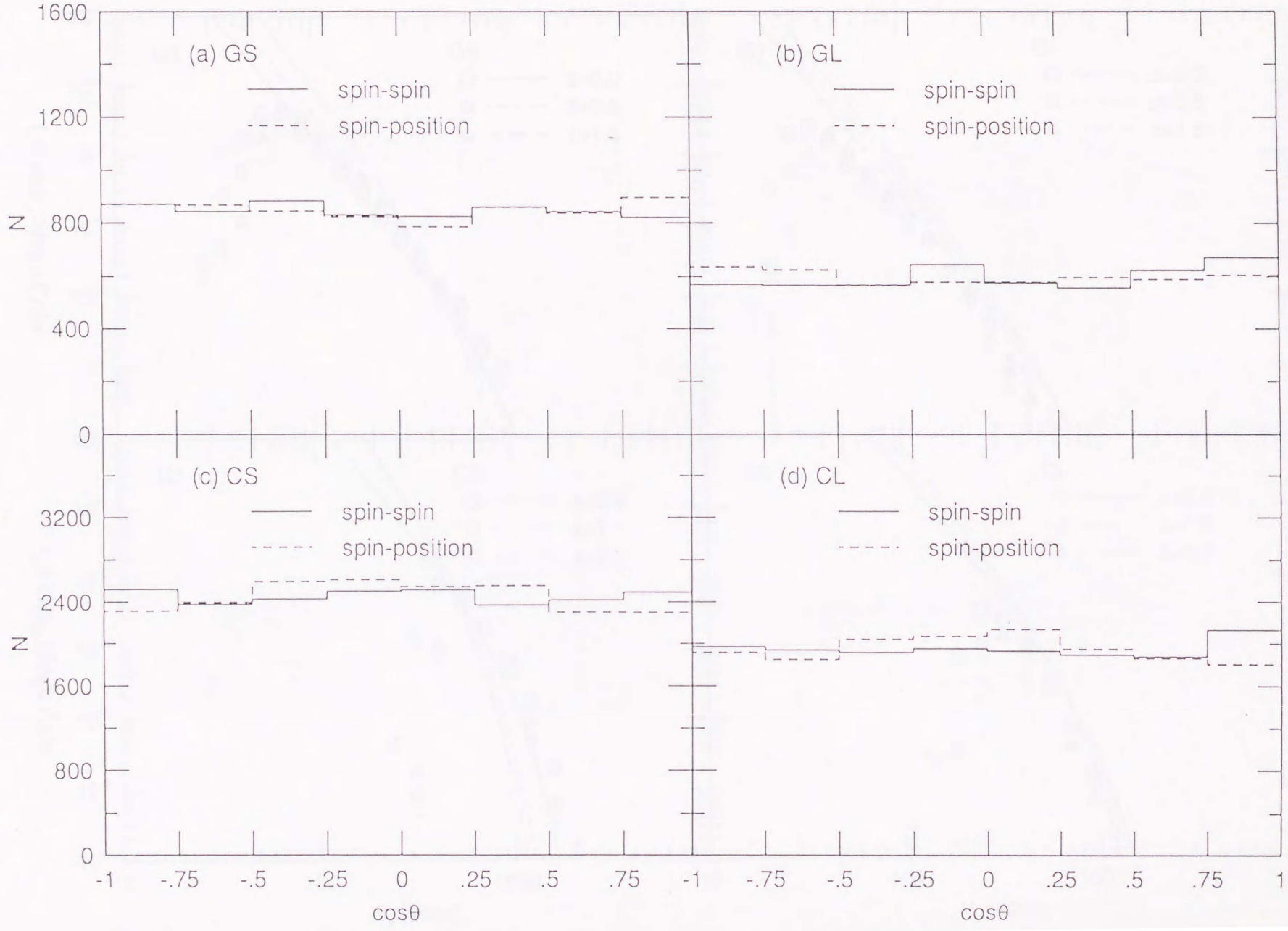
(a) GS
spin-spin
spin-position
(b) GL
spin-spin
spin-position
(c) CS
spin-spin
spin-position
(d) CL
spin-spin
spin-position
N
1600
1200
800
400
0
3200
2400
1600
800
0
-1
-.75
-.5
-.25
0
.25
.5
.75
1
cosθ

Figure 13

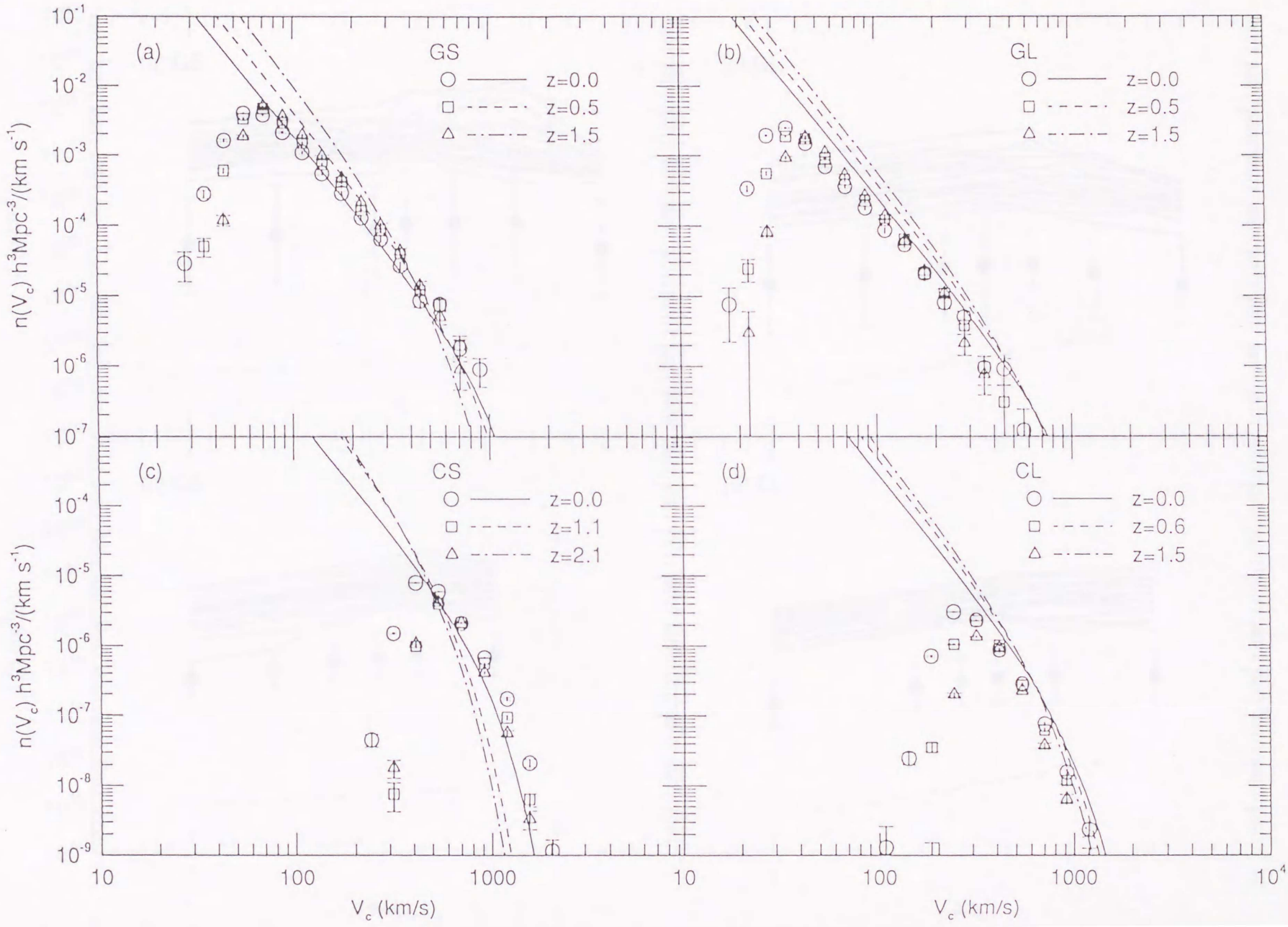
(a)
GS
z=0.0
z=0.5
z=1.5
(b)
GL
z=0.0
z=0.5
z=1.5
(c)
CS
z=0.0
z=1.1
z=2.1
(d)
CL
z=0.0
z=0.6
z=1.5
n(V_c) h^3Mpc^-3/(km s^-1)
V_c (km/s)
10
100
1000
10^4

Figure 14

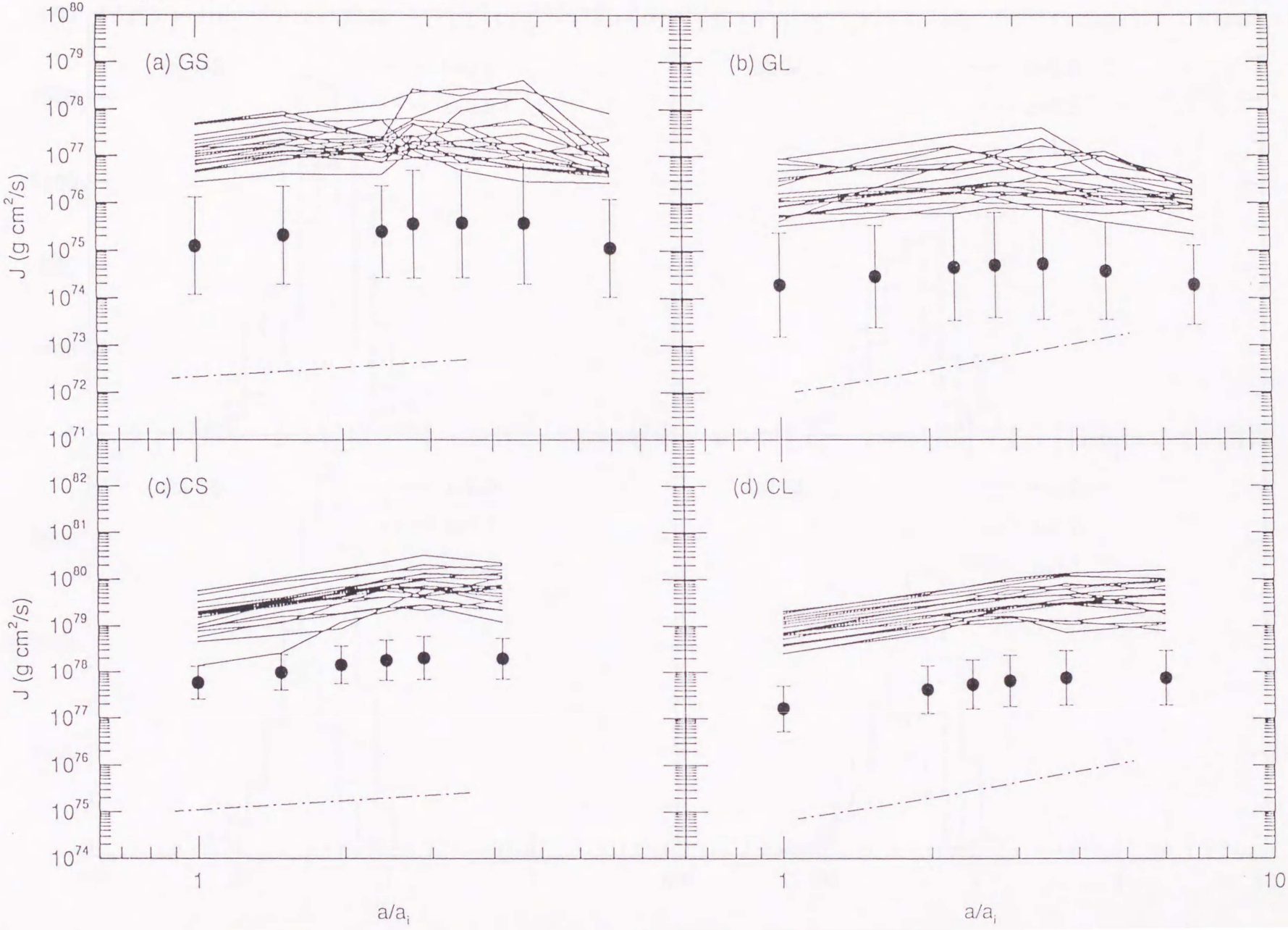
(a) GS
(b) GL
(c) CS
(d) CL
J (g cm²/s)
J (g cm²/s)
10⁸⁰
10⁷⁹
10⁷⁸
10⁷⁷
10⁷⁶
10⁷⁵
10⁷⁴
10⁷³
10⁷²
10⁷¹
10⁸²
10⁸¹
10⁸⁰
10⁷⁹
10⁷⁸
10⁷⁷
10⁷⁶
10⁷⁵
10⁷⁴
1
1
10
a/a_i
a/a_i

Figure 15

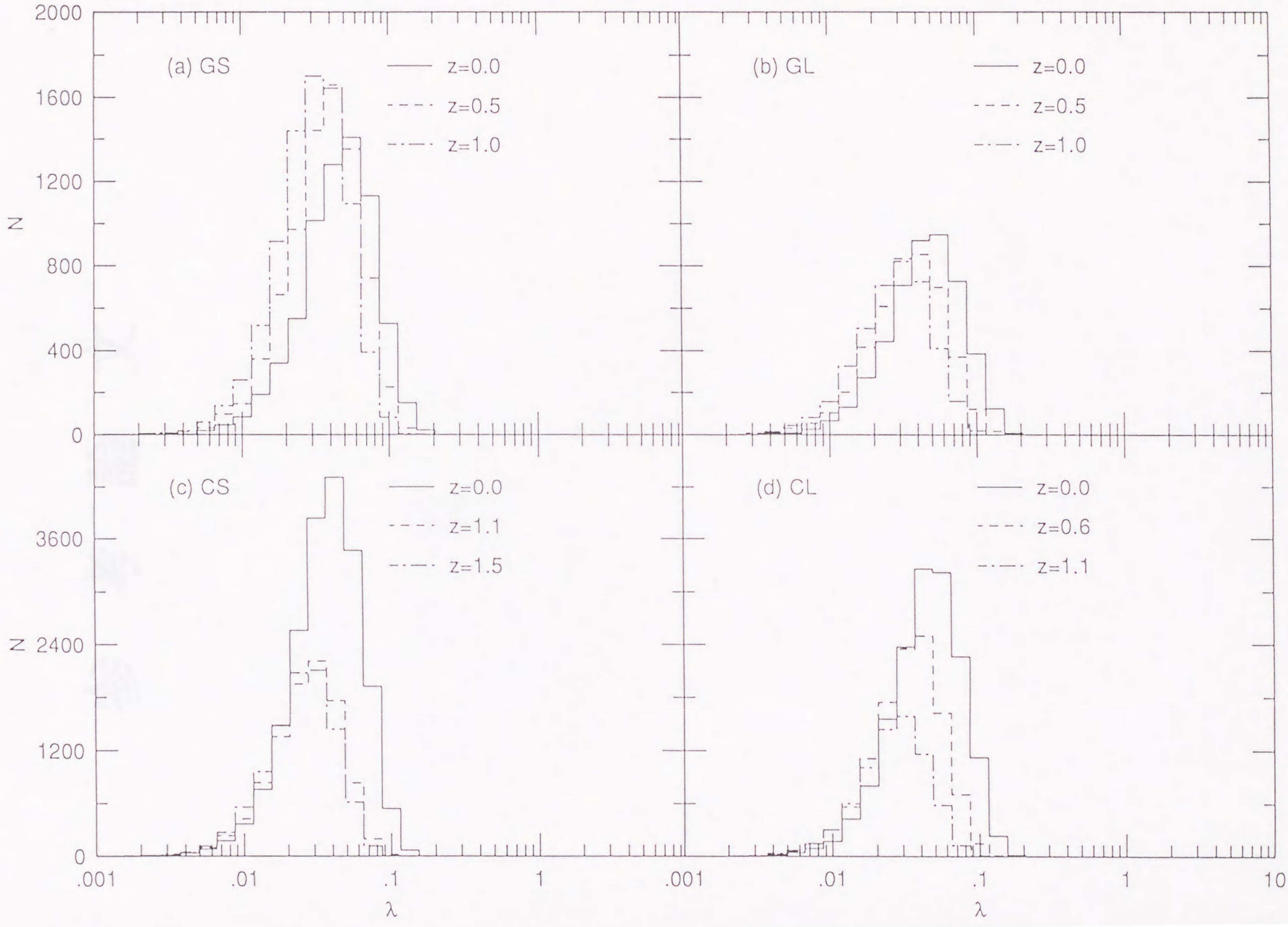
(a) GS
z=0.0
z=0.5
z=1.0
(b) GL
z=0.0
z=0.5
z=1.0
(c) CS
z=0.0
z=1.1
z=1.5
(d) CL
z=0.0
z=0.6
z=1.1
N
λ
2000
1600
1200
800
400
0
3600
2400
1200
.001
.01
.1
1
10